

1
2
3
4
5
6
7
8
9

This manuscript has been submitted for publication in RAPID COMMUNICATIONS IN MASS SPECTROMETRY. Please note that the manuscript has yet to undergo peer review or be formally accepted for publication. Subsequent versions of this manuscript may have slightly different content. If accepted, the final version of this manuscript will be available via the '*Peer-reviewed Publication DOI*' link on the right-hand side of this webpage. Please feel free to contact us — we welcome feedback.

10
11
12
13
14
15

16
17
18
19
20
21
22
23
24
25
26
27
28
29
30
31
32
33
34
35
36
37
38
39
40
41
42
43
44
45
46
47
48
49
50

In preparation for Rapid Communications in Mass Spectrometry
**pyisotopomer: A Python package for obtaining intramolecular isotope ratio differences
from mass spectrometric analysis of nitrous oxide isotopocules**

Colette L. Kelly,^{1*} Cara Manning,² Claudia Frey,³ Jan Kaiser,⁴ Noah Gluschkoff,¹ and Karen L. Casciotti

1. Stanford University, Department of Earth System Science, Stanford, CA 94305, USA
2. University of Connecticut, Department of Marine Sciences, Groton, CT, 06340, USA
3. Department of Environmental Science, University of Basel, Basel, Switzerland.
4. University of East Anglia, Centre for Ocean and Atmospheric Sciences, School of Environmental Sciences, Norwich, NR4 7TJ, UK

* **Correspondence to:** Colette L. Kelly (email: clkelly@stanford.edu; phone: 802-595-3647; address: 473 Via Ortega Room 140, Stanford, CA 94305).

Keywords: Nitrous oxide, isotopomers, isotopocules, scrambling, Python

Abstract

RATIONALE Obtaining nitrous oxide isotopocule measurements with isotope ratio mass spectrometry (IRMS) involves analyzing the ion current ratios of the nitrous oxide parent ion (N_2O^+) as well as those of the NO^+ fragment ion. The data analysis requires correcting for “scrambling” in the ion source, whereby the NO^+ fragment ion obtains the outer N atom from the N_2O molecule. While descriptions exist for this correction, and interlaboratory intercalibration efforts have been made, there has yet to be published a package of code for implementing isotopomer calibrations.

METHODS We developed a user-friendly Python package (pyisotopomer) to determine two coefficients (γ and κ) that describe scrambling in the IRMS ion source, and then to use this calibration to obtain intramolecular isotope deltas in N_2O samples.

RESULTS We show that, with two reference materials distinct enough in their site preference, γ and κ can be determined robustly and accurately for a given IRMS. An additional third reference material is needed to define the zero-point of the delta scale. We show that the scrambling behavior of an IRMS can vary with time, necessitating regular calibrations. Finally, we present an intercalibration between two IRMS laboratories, using pyisotopomer to calculate γ and κ , and to obtain intramolecular N_2O isotope deltas in lake water unknowns.

CONCLUSIONS Given these considerations, we discuss how to use pyisotopomer to obtain high-quality N_2O isotopocule data from IRMS systems, including the use of appropriate reference materials and frequency of calibration.

51 1. Introduction

52 Nitrous oxide (N₂O) is a potent greenhouse gas, with a global warming potential 265
53 times that of carbon dioxide over a 100 year time horizon^{1,2}. N₂O is also likely to be the most
54 emitted ozone depletion agent in the 21st century, due to production of NO radicals in the
55 stratosphere that interact destructively with ozone³⁻⁶. Historically, the bulk stable isotopes of
56 nitrogen and oxygen in N₂O have been used to quantify its microbial cycling in soils^{7,8} and in the
57 ocean⁹⁻¹², its destruction by photolysis and O(¹D), and its cycling in the atmosphere^{13,14}. This
58 approach often fails to provide a unique solution, because the bulk nitrogen and oxygen isotope
59 ratios of N₂O depend on the isotopic composition of the substrate, as well as the isotope effects
60 of production and consumption processes¹². Furthermore, in the context of microbial N₂O
61 cycling in soils and the ocean, bacterial nitrification and denitrification produce N₂O with similar
62 bulk $\delta(^{15}\text{N})^1$ values, preventing partitioning between these processes on the basis of bulk $\delta(^{15}\text{N})$
63 alone^{15,16}.

64 The site-specific nitrogen isotope ratios of N₂O provide a more nuanced constraint on the
65 biogeochemical cycling of N₂O than its bulk composition alone. N₂O isotopomers have been
66 used extensively to quantify its biogeochemical cycling in soils¹⁷⁻²⁰, the atmosphere^{14,21-23}, and
67 the ocean²⁴⁻³⁴. The individual isotopic compositions of each nitrogen atom were first measured
68 by Friedman and Bigeleisen, who quantified the yields of isotopomers ¹⁴N¹⁵N¹⁶O and ¹⁵N¹⁴N¹⁶O
69 from enriched ammonium nitrate by measuring the NO⁺ fragment ion signal in an isotope ratio
70 mass spectrometer (IRMS)³⁵. 50 years later, these N₂O isotopomers were quantified at natural
71 abundance from the N₂O⁺ species with mass numbers 44, 45, and 46 and the mass 30 and 31
72 NO⁺ fragment ion^{36,37}. The central nitrogen atom in the N₂O molecule has been designated with
73 locants α , μ , or 2; the terminal atom, with locants β , τ , or 1^{38,39}. Here, we use the definitions from
74 Toyoda and Yoshida (1999) for the site-specific isotope number (N) ratios of the central (α)
75 nitrogen atom and terminal (β) nitrogen atom³⁶:

$$^{15}R^{\alpha} = \frac{N(^{14}\text{N}^{15}\text{NO})}{N(^{14}\text{N}^{14}\text{NO})} \quad (1)$$

$$^{15}R^{\beta} = \frac{N(^{15}\text{N}^{14}\text{NO})}{N(^{14}\text{N}^{14}\text{NO})} \quad (2)$$

77
78 The N₂O isotopomer measurement was initially performed with two sequential
79 measurements of the same sample on an isotope ratio mass spectrometer, one at m/z 44, 45, and
80 46, and the other at m/z 30 and 31³⁶. Use of dedicated cup-configurations on lower-dispersion
81 IRMS instruments allowed simultaneous analysis of all five masses together⁴⁰.

82 The slight difference in absorption cross sections between the isotopocules of N₂O result
83 in different isotopic fractionations during photolysis and photo-oxidation in the stratosphere⁴¹,
84 making the isotopomers of N₂O a powerful tool for understanding its atmospheric cycling^{21,42-45}.
85 Likewise, N₂O site preference, defined as $\delta(^{15}\text{N}^{\text{sp}}) = \delta(^{15}\text{N}^{\alpha}) - \delta(^{15}\text{N}^{\beta})$, was shown in microbial
86 culture experiments to be largely a function of reaction mechanism, independent of source
87 composition^{24,46-50}. This allowed for the differentiation between N₂O from bacterial nitrification
88 and denitrification, although some debate exists about whether the site preference of N₂O
89 produced by denitrifying bacteria is closer to 0 ‰ or 25 ‰^{49,51}, the latter possibility being largely

¹ We write δ values with parentheses, e.g., $\delta(^{15}\text{N})$, because δ is the quantity symbol and “¹⁵N” is the label. See SI Brochure: <https://www.bipm.org/en/publications/si-brochure/>

90 ignored in subsequent literature. During N₂O consumption, $\delta(^{15}\text{N}^\alpha)$ and $\delta(^{18}\text{O})$ were shown in
 91 microbial culture⁵² and soil mesocosm¹⁹ experiments to exhibit a characteristic relationship,
 92 allowing subsequent studies to use this relationship to distinguish between oxidative and
 93 reductive regimes of N₂O cycling^{30,33}.

94 Site-specific nitrogen isotope ratio measurements based on mass spectrometry need to be
 95 corrected for a phenomenon called “scrambling,” whereby the NO⁺ fragment ion contains the
 96 terminal N atom, rather than the central N attached to the O atom (as in the original molecule). A
 97 number of approaches have been taken to calibrate an IRMS system for this effect: the use of a
 98 single “rearrangement factor” to describe scrambling^{36,53}, the use of nine coefficients to describe
 99 the different fragmentation behaviors of the different isotopocules of N₂O⁵⁴, and finally the use
 100 of two coefficients to describe scrambling in the ion source⁵⁰. While descriptions exist for each
 101 of these approaches, and interlaboratory intercalibration efforts have been made^{55,56}, there has yet
 102 to be published a package of code for implementing one of the above isotopomer calibrations.

103 We developed a Python software package that implements the two-coefficient approach
 104 described by Frame and Casciotti³² to calibrate an IRMS for scrambling and use that calibration
 105 to obtain high-quality N₂O isotopocule data. This software solves a set of equations, either
 106 analytically or with an optimization routine, to quantify the scrambling behavior of an IRMS. To
 107 quantify the performance of the software, we tested the sensitivity of the analytical and
 108 optimization-based solutions to their input conditions and assessed when each method is most
 109 appropriate. To quantify the variability of the fragmentation behavior of an instrument over time,
 110 we examined the scrambling behavior of one IRMS over the course of four years of
 111 measurements. We derived a simplified equation and used a Monte Carlo simulation approach to
 112 quantify the effect of uncertainty in the scrambling coefficients on the final isotope deltas.
 113 Finally, we performed an intercalibration using this software across two labs, at Stanford
 114 University (‘Lab 1’) and the University of Basel (‘Lab 2’).

115

116 2. Mathematical framework

117 The molecular ion number ratios 45/44 (⁴⁵R) and 46/44 (⁴⁶R) can be written in terms of
 118 atomic isotope ratios as^{36,53}:

$$45R = {}^{15}R^\alpha + {}^{15}R^\beta + {}^{17}R \quad (3)$$

$$46R = ({}^{15}R^\alpha + {}^{15}R^\beta){}^{17}R + {}^{18}R + {}^{15}R^\alpha{}^{15}R^\beta \quad (4)$$

119 where ¹⁵R^α, ¹⁵R^β, ¹⁷R and ¹⁸R denote the number ratios of ¹⁴N¹⁵N¹⁶O, ¹⁵N¹⁴N¹⁶O, ¹⁴N₂¹⁷O, and
 120 ¹⁴N₂¹⁸O, respectively, to ¹⁴N₂¹⁶O, assuming a stochastic isotope distribution between mono- and
 121 poly-substituted isotopocules.

122 For many N₂O samples, ¹⁷R covaries with ¹⁸R according to the oxygen isotope ratios of
 123 Vienna Standard Mean Ocean Water (VSMOW)^{57,58} and a mass-dependent relationship between
 124 ¹⁷R and ¹⁸R with coefficient $\beta = 0.516$ ⁵⁹. Deviations from this relationship are expressed by the
 125 oxygen triple isotope excess $\Delta(^{17}\text{O})$ ^{59–61}, which provides additional information about the sources
 126 and sinks of N₂O^{59,62}:

$${}^{17}R/{}^{17}R_{\text{VSMOW}} = ({}^{18}R/0.0020052)^\beta [\Delta(^{17}\text{O}) + 1] \quad (5)$$

127

128 The simplest formulation for the NO⁺ fragment ion number ratio 31/30 (³¹R) is given as¹⁸:

$${}^{31}R = {}^{15}R^\alpha + {}^{17}R \quad (6)$$

129 This equation would represent the ^{31}R measured by IRMS if no scrambling occurred.

130 To describe instead the scrambled ^{31}R , Toyoda and Yoshida¹⁸ define the rearrangement
131 factor γ (which was later given the symbol γ) as “the fraction of NO^+ bearing the β nitrogen of
132 the initial N_2O to the total NO^+ formed,” to yield:

$$^{31}R = (1 - \gamma)^{15}R^\alpha + \gamma^{15}R^\beta + ^{17}R \quad (7)$$

133 where $^{15}R^\alpha$ and $^{15}R^\beta$ represent atomic isotope ratios of the sample. In other words, γ relates the
134 scrambled NO^+ fragment ratio to the unscrambled $^{15}R^\alpha$ and $^{15}R^\beta$ of the sample.

135 Kaiser et al.⁵⁵ introduced a more complete representation of ^{31}R , adding terms for
136 $^{15}\text{N}^{15}\text{N}^{16}\text{O}$, $^{14}\text{N}^{15}\text{N}^{17}\text{O}$, and $^{15}\text{N}^{14}\text{N}^{17}\text{O}$ to m/z 31, and terms for $^{15}\text{N}^{14}\text{N}^{16}\text{O}$ and $^{14}\text{N}^{15}\text{N}^{16}\text{O}$ to m/z
137 30:

$$\begin{aligned} ^{31}R &= (1 - \gamma)^{15}R^\alpha + \gamma^{15}R^\beta + ^{17}R - \frac{\gamma(1 - \gamma)(^{15}R^\alpha - ^{15}R^\beta)^2}{1 + \gamma^{15}R^\alpha + (1 - \gamma)^{15}R^\beta} \quad (8) \\ &= \frac{(1 - \gamma)^{15}R^\alpha + \gamma^{15}R^\beta + ^{15}R^\alpha^{15}R^\beta + ^{17}R[1 + \gamma^{15}R^\alpha + (1 - \gamma)^{15}R^\beta]}{1 + \gamma^{15}R^\alpha + (1 - \gamma)^{15}R^\beta} \end{aligned}$$

138 Note that Kaiser et al.⁵⁵ use the symbol “ s ” for γ , $^{15}R_1$ for $^{15}R^\beta$, and $^{15}R_2$ for $^{15}R^\alpha$.

139 To account for different fragmentation rates of different N_2O isotopocules, Westley et
140 al.⁵² replaced the rearrangement factor γ with nine separate coefficients:

$$^{31}R = \frac{a_{31}^{15}R^\alpha + b_{31}^{15}R^\beta + c_{31}^{15}R^\alpha^{15}R^\beta + ^{17}R[d_{31} + e_{31}^{15}R^\alpha + f_{31}^{15}R^\beta]}{1 + a_{30}^{15}R^\alpha + b_{30}^{15}R^\beta + c_{30}^{15}R^\alpha^{15}R^\beta} \quad (9)$$

141 While this approach considers the possibility of different rearrangement factors for every
142 N_2O isotopocule as well as $^{15}\text{N}_2^+$ formation, it also requires solving for three to nine coefficients,
143 depending on whether a_{30} , b_{30} and c_{30} , as well as d_{31} , e_{31} and f_{31} , are considered separately from
144 coefficients a_{31} , b_{31} and c_{31} .

145 Frame and Casciotti³² simplify this equation by reducing the number of rearrangement
146 factors to two coefficients, γ and κ , which represent the yield of $^{14}\text{NO}^+$ from $^{14}\text{N}^{15}\text{N}^{16}\text{O}$ and
147 $^{14}\text{N}^{15}\text{N}^{17}\text{O}$, and the yield of $^{15}\text{NO}^+$ from $^{15}\text{N}^{14}\text{N}^{16}\text{O}$, respectively. This produces the equation:
148

$$^{31}R = \frac{(1 - \gamma)^{15}R^\alpha + \kappa^{15}R^\beta + ^{15}R^\alpha^{15}R^\beta + ^{17}R[1 + \gamma^{15}R^\alpha + (1 - \kappa)^{15}R^\beta]}{1 + \gamma^{15}R^\alpha + (1 - \kappa)^{15}R^\beta} \quad (10)$$

149 The important pieces of information contained within the two scrambling factors are the
150 unequal rates of fragmentation for the isotopomers $^{14}\text{N}^{15}\text{NO}$ and $^{15}\text{N}^{14}\text{NO}$, which eqns. (7) and
151 (8) assume are equal. Eqn. (10) is formulated by assuming that the ^{17}O -isotopocules have the
152 same scrambling behavior as the ^{16}O -isotopocules, i.e., $e_{31} = 1 - a_{31}$ and $f_{31} = 1 - b_{31}$, in terms of
153 the coefficients in eqn. 9. It is also assumed that $c_{31} = 1$, i.e., the yield of $^{15}\text{N}^{16}\text{O}^+$ from $^{15}\text{N}_2^{16}\text{O}$ is
154 equal to the yield of $^{14}\text{N}^{16}\text{O}^+$ from $^{14}\text{N}_2^{16}\text{O}$. Given that naturally occurring N_2O contains very
155 little $^{15}\text{N}_2^{16}\text{O}$, a small difference in this yield would not significantly alter ^{31}R ⁶³. Finally, it is
156 assumed that $d_{31} = 1$, or that the yield of $^{14}\text{N}^{17}\text{O}^+$ from $^{14}\text{N}_2^{17}\text{O}$ is equal to the yield of $^{14}\text{N}^{16}\text{O}^+$
157 from $^{14}\text{N}_2^{16}\text{O}$; again, an assumption yielding little error in ^{31}R , given the low natural abundance
158 of ^{17}O in N_2O ⁵⁹.

159 Eqn. (10) can be rearranged to give an equation for γ as a function of κ (the full
160 derivation is presented in Supplementary text S1):

$$\gamma = \frac{^{15}R^\alpha + \kappa^{15}R^\beta + ^{15}R^\alpha^{15}R^\beta - (^{31}R - ^{17}R)[1 + (1 - \kappa)^{15}R^\beta]}{^{15}R^\alpha(1 + (^{31}R - ^{17}R))} \quad (11)$$

161 For two reference materials, we can write two such equations and solve for two
 162 unknowns, γ and κ . $^{15}R^\alpha$ and $^{15}R^\beta$ represent *known* values for each reference material, and ^{31}R is
 163 the observed quantity. Essentially, we are asking what values of γ and κ for a pair of known $^{15}R^\alpha$
 164 and $^{15}R^\beta$ values gives the observed ^{31}R for each reference gas. Setting the two solutions for γ
 165 equal allows us to determine κ and γ algebraically from the assigned ^{15}R values of reference
 166 materials 1 and 2 ($^{15}R_1^\alpha$, $^{15}R_1^\beta$, $^{15}R_2^\alpha$, $^{15}R_2^\beta$), their observed ^{31}R values ($^{31}R_1$, $^{31}R_2$), and the ^{17}R
 167 values ($^{17}R_1$, $^{17}R_2$):

$$\kappa = \frac{\frac{(^{15}R_1^\alpha - ^{31}R_1 + ^{17}R_1)(1 + ^{15}R_1^\beta)}{^{15}R_1^\alpha(1 + ^{31}R_1 - ^{17}R_1)} - \frac{(^{15}R_2^\alpha - ^{31}R_2 + ^{17}R_2)(1 + ^{15}R_2^\beta)}{^{15}R_2^\alpha(1 + ^{31}R_2 - ^{17}R_2)}}{\frac{^{15}R_2^\beta}{^{15}R_2^\alpha} - \frac{^{15}R_1^\beta}{^{15}R_1^\alpha}} \quad (12a)$$

$$\gamma = \frac{\frac{(^{15}R_1^\alpha - ^{31}R_1 + ^{17}R_1)(1 + ^{15}R_1^\beta)}{^{15}R_1^\alpha(1 + ^{31}R_1 - ^{17}R_1)} \left(\frac{^{15}R_2^\beta}{^{15}R_2^\alpha}\right) - \frac{(^{15}R_2^\alpha - ^{31}R_2 + ^{17}R_2)(1 + ^{15}R_2^\beta)}{^{15}R_2^\alpha(1 + ^{31}R_2 - ^{17}R_2)} \left(\frac{^{15}R_1^\beta}{^{15}R_1^\alpha}\right)}{\frac{^{15}R_2^\beta}{^{15}R_2^\alpha} - \frac{^{15}R_1^\beta}{^{15}R_1^\alpha}} \quad (12b)$$

168 After substituting $^{45}R - ^{15}R^\alpha - ^{15}R^\beta$ for ^{17}R , the equations for γ and κ can also be written as
 169 follows:

$$\kappa = \frac{\frac{(^{45}R_1 - ^{31}R_1 - ^{15}R_1^\beta)(1 + ^{15}R_1^\beta)}{^{15}R_1^\alpha(1 + ^{15}R_1^\alpha + ^{15}R_1^\beta + ^{31}R_1 - ^{45}R_1)} - \frac{(^{45}R_2 - ^{31}R_2 - ^{15}R_2^\beta)(1 + ^{15}R_2^\beta)}{^{15}R_2^\alpha(1 + ^{15}R_2^\alpha + ^{15}R_2^\beta + ^{31}R_2 - ^{45}R_2)}}{\frac{^{15}R_2^\beta}{^{15}R_2^\alpha} - \frac{^{15}R_1^\beta}{^{15}R_1^\alpha}} \quad (13a)$$

$$\gamma = \frac{\frac{(^{45}R_1 - ^{31}R_1 - ^{15}R_1^\beta)(1 + ^{15}R_1^\beta)}{^{15}R_1^\alpha(1 + ^{15}R_1^\alpha + ^{15}R_1^\beta + ^{31}R_1 - ^{45}R_1)} \left(\frac{^{15}R_2^\beta}{^{15}R_2^\alpha}\right) - \frac{(^{45}R_2 - ^{31}R_2 - ^{15}R_2^\beta)(1 + ^{15}R_2^\beta)}{^{15}R_2^\alpha(1 + ^{15}R_2^\alpha + ^{15}R_2^\beta + ^{31}R_2 - ^{45}R_2)} \left(\frac{^{15}R_1^\beta}{^{15}R_1^\alpha}\right)}{\frac{^{15}R_2^\beta}{^{15}R_2^\alpha} - \frac{^{15}R_1^\beta}{^{15}R_1^\alpha}} \quad (13b)$$

171 To obtain $^{31}R_1$ and $^{31}R_2$ in continuous-flow analysis, we measure two reference materials
 172 against a common working reference gas (wr), which is calibrated independently. The working
 173 reference is a third calibrated reference material that normalizes different runs to the same
 174 reference frame:
 175

$$^{31}R_1 = (1 + ^{31}\delta_1)^{31}R_{wr} \quad (14)$$

$$^{31}R_2 = (1 + ^{31}\delta_2)^{31}R_{wr} \quad (15)$$

176 where $^{31}R_1$ and $^{31}R_2$ are calculated values that depend on γ and κ ; $^{31}\delta$ is the measured ion
 177 current ratio difference of sample (1 or 2) to working reference peak, and $^{31}R_{wr}$ is an assumed

178 value calculated with constant γ and κ and assigned $^{15}R^\alpha$, $^{15}R^\beta$, and ^{17}R . Calculating $^{31}R_{wr}$ with
179 constant γ and κ assumes that the working reference peak experiences a defined scrambling
180 behavior that could differ from that of a sample peak; ultimately, however, $^{31}R_{wr}$ drops out of the
181 final $\delta(^{15}N^{sp})$ calculation, so this assumption has little effect.

182 The “algebraic” solution in pyisotopomer⁶⁴ uses $^{31}R_1$ and $^{31}R_2$ in eqns. (11) and (12) to
183 obtain γ and κ . The “least_squares” method in pyisotopomer⁶⁴ solves eqns. (14) and (15) for γ
184 and κ iteratively with a least squares optimization routine. We present a full discussion of the
185 appropriate use of the algebraic and least squares methods in section 4.2.

186 Some of the isotopomer literature obtains $^{15}R^{bulk}$ and $^{15}R^\alpha$ by regression between true and
187 measured values of reference materials, inferring $^{15}R^\beta$ indirectly²⁰. In this case, a linear
188 calibration curve replaces the scrambling correction. A linear calibration curve is only acceptable
189 if the unknowns are close in their $\delta(^{15}N^{sp})$ to those of the reference material — although in this
190 case, it may not even be necessary to use a more than one reference material. It is not accurate if
191 unknowns diverge in their $\delta(^{15}N^{sp})$ from that of the reference material(s). This is because the
192 measured $^{31}\delta$ value depends on both $^{15}R^\alpha$ and $^{15}R^\beta$ (Supplementary text S2).

193 To obtain $^{15}R^\alpha$, $^{15}R^\beta$, and ^{18}R of unknowns, pyisotopomer solves for these values from
194 eqns. (3), (4), (5), and (10), using ^{31}R , ^{45}R , ^{46}R , γ , and κ as input terms⁵⁰. The delta values $\delta(^{15}N^\alpha)$,
195 $\delta(^{15}N^\beta)$, $\delta(^{15}N^{sp})$, $\delta(^{15}N^{bulk})$, and $\delta(^{18}O)$ are calculated from $^{15}R^\alpha$, $^{15}R^\beta$, and ^{18}R relative to primary
196 reference scales (^{15}R from atmospheric N_2 and ^{18}R from VSMOW; if desired, the values of
197 primary reference scale ratios may be adjusted with keyword arguments, as described in the
198 pyisotopomer Documentation⁶⁴). Additionally, if $\Delta^{17}O$ has been measured separately^{59,61,62},
199 pyisotopomer can take this value into account in the calculation of $\delta(^{15}N^\alpha)$, $\delta(^{15}N^\beta)$, $\delta(^{15}N^{sp})$,
200 $\delta(^{15}N^{bulk})$, and $\delta(^{18}O)$.

201

202 3. Experimental methods

203 3.1 Preparation and analysis of dissolved N_2O reference materials

204 A series of dissolved N_2O reference materials (Table 1) were prepared and analyzed in
205 both Lab 1 and Lab 2. Reference materials were prepared by filling 160-mL glass serum bottles
206 (Wheaton) with de-ionized water and removing a 4-mL headspace (Lab 1) or 10 to 20-mL
207 headspace (Lab 2), then capped with a gray butyl rubber septum (National Scientific) and sealed
208 with an aluminum crimp seal. These bottles were purged with helium for 90 minutes at yields a
209 minimum flow rate of 100 mL/min to remove all background N_2O . The purged bottles were then
210 injected with 2 to 43 nmol N_2O (Lab 1) or 1 to 60 nmol N_2O (Lab 2) in a matrix of He or
211 synthetic air (Table 1) using a gas-tight syringe. Reference materials prepared in Lab 1 were
212 preserved with 100 μ L saturated mercuric chloride ($HgCl_2$) solution; those prepared in Lab 2
213 contained no added preservative. For Lab 1, atmosphere-equilibrated seawater was prepared by
214 filtering surface seawater (collected in Half Moon Bay, CA) through a 0.22 mm Sterivex filter,
215 allowing it to undergo static equilibration with outdoor air for three days, then re-filtering into
216 160-mL serum bottles, removing a 1-mL headspace, and preserving with 100 μ L saturated
217 mercuric chloride solution. For Lab 2, atmosphere-equilibrated reference materials were
218 prepared by purging either de-ionized water or a sodium chloride solution with helium, allowing
219 it to undergo static equilibration with outdoor air for three days, filling into 160-mL serum
220 bottles, and removing a 10-mL headspace. Reference materials were run in the same format as
221 samples to account for any potential fractionation associated with the purge-and-trap system. The
222 magnitude of such fractionation was quantified for Lab 1 by running aliquots of the pure N_2O
223 reference tank in sample format; this test yielded offsets of (0.22 ± 0.52) ‰ for $\delta(^{15}N^{bulk})$ and

224 (0.16±0.62) ‰ for $\delta(^{18}\text{O})$ vs. the reference tank injection (see Supplementary text S3 for a full
225 discussion of potential fractionation effects in the purge-and-trap system).

226 The reference gases were calibrated independently by J. Mohn (EMPA; mini-QCLAS
227 aerodyne) or S. Toyoda (Tokyo Tech; IRMS), except for one internal standard used by Lab 1
228 (B6; Table 1). The $\delta(^{17}\text{O})$ values for each gas were calculated assuming a mass-dependent
229 relationship between ^{17}R and ^{18}R (eqn. 5).

230 Reference gases and samples were measured on Thermo Finnigan DELTA V Plus isotope
231 ratio mass spectrometers (IRMS; Thermo Fisher Scientific, Waltham, MA) in Labs 1 and 2. Each
232 IRMS had Faraday cups configured to simultaneously measure m/z 30, 31, 44, 45, and 46.
233 Reference materials and samples were analyzed on custom purge-and-trap systems coupled to
234 each IRMS, which was run in continuous flow mode⁶⁵ (Table 1). The two systems had slight
235 differences in the purge-and-trap method: in Lab 1, liquid from each sample bottle was
236 transferred under helium pressure to a sparging column to extract the dissolved gases⁶⁶; in Lab 2,
237 each sample was extracted by purging directly from the bottle. The effects of these differences
238 are discussed further in Results and Discussion.

239

240 3.2 Data corrections

241 3.2.1 Linearity relation

242 The measured ion current ratios 31/30, 45/44, and 46/44 of each sample peak were
243 divided by those of the working reference peak. This produced three molecular isotope delta
244 values $^{31}\delta+1$, $^{45}\delta+1$, and $^{46}\delta+1$, where $\delta = R_s/R_{wr} - 1$, with the subscripts “s” and “wr” denoting
245 sample and working reference, respectively (Figure 1, Step 5).

246 The δ values were corrected for the effect of peak size³³. For Lab 1, this was
247 accomplished by running six reference materials (reference gases S2, B6, A01, CA06261, 90454,
248 and 94321; Table 1) in size series ranging from 2-43 nmol N₂O. For Lab 2, three reference
249 materials (CA06261, 53504, and CA08214) were run in size series ranging from 1-60 nmol N₂O
250 (Figure 1, Step 6).

251 To obtain a single size correction slope from multiple size series, we used the dummy-
252 variable method of combining regressions⁶⁷. The dummy variable method is an improvement
253 over simply averaging each individually calculated slope because it implicitly weighs each size
254 series by its informativeness, producing a slope that is more likely to reflect the overall linearity
255 behavior of the instrument⁶⁷. For a given material, each measured $\delta+1$ is a linear function of its
256 peak area (A) plus an intercept ($\gamma_1 + \gamma_2 D_2 + \gamma_3 D_3$):

$$\delta + 1 = \hat{\beta}A + \gamma_1 + \gamma_2 D_2 + \gamma_3 D_3 \quad (16)$$

257 where $\hat{\beta}$ represents the regression coefficient for a particular peak area (for m/z 31,45, or 46),
258 obtained by multiple linear regression. The intercept for reference material 1 is γ_1 . D_2 and D_3 are
259 ‘dummy variables’ to adjust γ_1 by an appropriate intercept for reference material 2 ($\gamma_1 + \gamma_2$) and
260 reference material 3 ($\gamma_1 + \gamma_3$). Thus, for reference material 1, $D_2 = D_3 = 0$; for reference material
261 2, $D_2 = 1$ and $D_3 = 0$; for reference material 3, $D_2 = 0$ and $D_3 = 1$. These dummy variables allow
262 us to obtain one slope for each isotope delta from multiple datasets accounting for differences in
263 intercept, with each reference material weighted by its spread in the x -axis range. Thus, slopes
264 $\hat{\beta}_{31}$, $\hat{\beta}_{45}$, and $\hat{\beta}_{46}$ were calculated for $^{31}\delta+1$, $^{45}\delta+1$, and $^{46}\delta+1$, respectively, each using eqn. (16).

265 To normalize measured values of $\delta+1$ to a common peak area, we first calculated the
266 $(\delta+1)_0$ that would be measured at m/z 44 peak area A_0 :

$$(\delta + 1)_0 = \hat{\beta}(A_0) + \gamma_1 + \gamma_2 D_2 + \gamma_3 D_3 \quad (17)$$

267 Note that $(\delta+1)_0$ is still a function of $\hat{\beta}$, the intercepts $\gamma_1, \gamma_2, \gamma_3$, and the dummy variables D_2 and
 268 D_3 . To obtain the difference $\delta_0 - \delta$ from the measured m/z 44 peak area A , we subtract eqn. (17)
 269 from eqn. (16), to obtain:

$$(\delta + 1)_0 - (\delta + 1) = \hat{\beta}(A_0 - A)$$

270 In this case, the size-corrected molecular isotope ratio, δ_0 , for each sample with measured δ and
 271 peak area A is given by:

$$(\delta + 1)_0 = \hat{\beta}(A_0 - A) + (\delta + 1) \quad (18)$$

272 Eqn. (18) is simply a function of the slope $\hat{\beta}$, the measured (A) and target (A_0) m/z 44 peak areas,
 273 and the measured δ . Thus, eqn. (18) can be applied across a range of peak areas and δ values to
 274 normalize these δ values to a common peak area. Using this method, we normalized the
 275 measured $^{31}\delta+1$, $^{45}\delta+1$, and $^{46}\delta+1$ of each sample to a peak area (A_0) of 20 Vs (Figure 1, Step 7).
 276

277 3.2.2 Scale normalization and calculation of ^{17}R

278 After applying the linearity correction, a scale normalization was applied to $^{45}\delta$ and $^{46}\delta$
 279 (Figure 1, Step 8). The scale normalization for $^{45}\delta$ and $^{46}\delta$ needs to be carried out before the
 280 scrambling correction (which is essentially a scale normalization of $^{31}\delta$); otherwise, the wrong
 281 bulk $^{15}\text{N}/^{14}\text{N}$ and $^{18}\text{O}/^{16}\text{O}$ ratios are implied. Furthermore, while the γ and κ calculations
 282 constrain the differences between $\delta(^{15}\text{N}^\alpha)$ and $\delta(^{15}\text{N}^\beta)$, their absolute values are governed by
 283 $\delta(^{15}\text{N}^{\text{bulk}})$, necessitating that the “correct”, normalized value of $^{45}\delta$ be input to the scrambling
 284 equations. This scale normalization is a replacement for any scale normalization or offset
 285 correction to the final output δ values, such as the one-point and two-point offset corrections
 286 calculated and applied in Mohn et al. (2014).

287 A scale normalization was calculated for each run included in the intercalibration
 288 exercise. Since assigned values of ^{45}R and ^{46}R for each reference gas were unavailable, assigned
 289 ^{45}R and ^{46}R were calculated from assigned $^{15}R^\alpha$, $^{15}R^\beta$, and ^{18}R and eqns. (3), (4), and (5) (Table
 290 1), assuming $^{17}R_{\text{VSMOW}} = 0.0003799^{68}$ and $^{18}R_{\text{VSMOW}} = 0.0020052^{57}$. Next, the assigned ^{45}R and
 291 ^{46}R for each reference gas were divided by the known ^{45}R and ^{46}R of the direct N_2O reference
 292 injection to obtain assigned $^{45}\delta$ and $^{46}\delta$ for each reference material. Then, these assigned $^{45}\delta$ and
 293 $^{46}\delta$ values were compared to measured $^{45}\delta$ and $^{46}\delta$ values, and scale normalization coefficients
 294 were calculated following the logarithmic scale normalization outlined in Kaiser et al. (2007):

$$\ln(1 + ^{45}\delta^n) = m \ln(1 + ^{45}\delta) + b$$

296 where $^{45}\delta^n$ is the normalized $^{45}\delta$, “ m ” is the slope of the regression of $\ln(1+^{45}\delta^n)$ vs.
 297 $\ln(1+^{45}\delta)$, and “ b ” is the intercept (and likewise for $^{46}\delta$). From this regression, the normalized δ
 298 values can be obtained:

$$1 + ^{45}\delta^n = e^b(1 + ^{45}\delta)^m \quad (19)$$

299 For the working reference, the values of $^{45}\delta$ and $^{45}\delta^n$ are equal to zero, so the intercept b
 300 should be equal to or very close to zero. The benefit of the logarithmic normalization is that,
 301 unlike a linear scale normalization, it is scale-invariant⁶¹: essentially, the logarithmic scale
 302 normalization does not skew the data towards extremely high or low values, and instead equally
 303 weights all data points⁶¹.

304 Next, a measured ^{18}R was derived from the scale-normalized ^{45}R and ^{46}R for each sample
 305 and reference material (Figure 1, Step 8). The size correction and scale normalization were
 306 carried out in the pyisotopomer spreadsheet template; the ^{18}R derivation from the scale-
 307 normalized ^{45}R and ^{46}R was the first step accomplished by the pyisotopomer code⁶⁴. Deriving ^{18}R

308 was accomplished by assuming a mass-dependent relationship between ^{17}R and ^{18}R (eqn. 5) and
 309 $^{15}R^\alpha = ^{15}R^\beta = ^{15}R^{\text{bulk}}$. These terms are then substituted into eqns. (3) and (4) to yield:

$$^{45}R = 2^{15}R^{\text{bulk}} + ^{17}R_{\text{VSMOW}} \left(\frac{^{18}R}{^{18}R_{\text{VSMOW}}} \right)^\beta (\Delta^{17}\text{O} + 1) \quad (20)$$

$$^{46}R = ^{18}R + 2^{15}R^{\text{bulk}} \left[^{17}R_{\text{VSMOW}} \left(\frac{^{18}R}{^{18}R_{\text{VSMOW}}} \right)^\beta (\Delta^{17}\text{O} + 1) \right] + (^{15}R^{\text{bulk}})^2 \quad (21)$$

310 Note that the slope β of the mass-dependent relationship between ^{17}R and ^{18}R is an
 311 adjustable parameter in the code (default: 0.516), and $\Delta^{17}\text{O}$ for each reference material may be
 312 entered in the data correction template and subsequently accounted for in this correction (default:
 313 0 ‰). Eqns. (20) and (21) were then solved for ^{18}R and $^{15}R^{\text{bulk}}$ to obtain an estimated ^{18}R and
 314 $^{15}R^{\text{bulk}}$ for each sample and reference material, and ^{17}R was calculated from ^{18}R according to eqn.
 315 (5). The resulting ^{18}R , ^{17}R , and $^{15}R^{\text{bulk}}$ were used in the scrambling calculation. They contain an
 316 error due to the assumption that $^{15}R^\alpha = ^{15}R^\beta = ^{15}R^{\text{bulk}}$, although the magnitude of this error should
 317 be small⁶¹. Later, the isotopomer calculation solves for $^{15}R^\alpha$ and $^{15}R^\beta$ separately and thus corrects
 318 this error.

319 In the intercalibration exercise, values of m and b were calculated from the slopes of
 320 assigned $^{45}\delta^a$ vs. measured $^{45}\delta$ and assigned $^{46}\delta^a$ vs. measured $^{46}\delta$ from the reference materials in
 321 each run. These runs took place in February 2021 for Lab 1 and August 2020 and November
 322 2020 for Lab 2. Combined, the scale normalization and size correction should account for any
 323 size- or isotope-ratio dependent effects, including those of a blank, linearity, or fractionation in
 324 the GasBench.

3.2.3 Calculating $^{31}R_m$ of the direct N₂O reference injection

327 We used the same scrambling coefficients for the working reference gas as for the
 328 samples. We recommend that the user calculates the ^{31}R of the direct reference injection ($^{31}R_{\text{wr}}$ in
 329 eqns. 14 and 15) with the following sequence of steps: 1) calculate $^{31}R_{\text{wr}}$ from eqn. (10) with
 330 either $\gamma = \kappa = 0.1$ or an *a priori* estimate, if available (Figure 1, Step 9); 2) use that $^{31}R_{\text{wr}}$ to
 331 correct data from two reference materials and from those reference materials, obtain γ and κ from
 332 eqns. (11) and (12) (Figure 1, Step 10); 3) use these updated γ and κ to re-calculate $^{31}R_{\text{wr}}$ from
 333 eqn. (10) (Figure 1, Step 11). The input γ and κ (used to calculate $^{31}R_{\text{wr}}$) and output γ and κ
 334 (calculated from paired reference materials) should converge quickly, so one iteration of this
 335 process should be sufficient. This value of $^{31}R_{\text{wr}}$ can then be used to convert $^{31}\delta$ to $^{31}R_s$. The user
 336 should also note that there are likely to be multiple pairings of input and output γ and κ that will
 337 consistently yield indistinguishable delta values.

3.2.4 IRMS scrambling calibration and isotopomer calculation

340 The "Scrambling" function of pyisotopomer was used to calculate γ and κ algebraically
 341 from all possible pairings of reference materials CA08214 and 53504 measured on a given IRMS
 342 (Lab 1 or Lab 2; Figure 1, Step 13). The reference materials CA08214 and 53504 were chosen
 343 because of their 113 ‰ $\delta(^{15}\text{N}^{\text{sp}})$ difference (see Results and Discussion for a description of how
 344 to choose reference material pairings), as well as the range of $\delta(^{15}\text{N}^\alpha)$, $\delta(^{15}\text{N}^\beta)$, $\delta(^{15}\text{N}^{\text{bulk}})$, and
 345 $\delta(^{18}\text{O})$ spanned by the two reference materials, which represent values found typically in
 346 culture^{52,69} and nature^{26,31}. One-week running averages of γ and κ were calculated to smooth their
 347 variation and used to obtain position-dependent δ values for unknowns and reference materials

348 run as unknowns for quality control (CA06261, S2, B6, and atmosphere-equilibrated seawater),
349 using the "Isotopomers" function of pyisotopomer (Figure 1, Step 14).

350 For comparison, this exercise was repeated, calculating γ and κ iteratively with the least
351 squares optimization (Figure 1, Step 12). The mean algebraic γ and κ from the paired reference
352 materials CA08214 and 53504 was used as the initial guess for the least squares solver. In this
353 case, reference materials CA08214 and CA06261 were used to calculate the least squares γ and
354 κ , because these reference materials are close in their calibrated isotopomer values to natural
355 abundance unknowns. As above, γ and κ were combined into a one-week running average; these
356 running averages of γ and κ for each system were used to obtain position-dependent δ values for
357 reference materials and unknowns in the intercalibration exercise (Figure 1, Step 14). The
358 analytical precisions of $\delta(^{15}\text{N}^\alpha)$, $\delta(^{15}\text{N}^\beta)$, $\delta(^{15}\text{N}^{\text{sp}})$, $\delta(^{15}\text{N}^{\text{bulk}})$, and $\delta(^{18}\text{O})$ produced by each method
359 are presented in the Results and Discussion.

360 N_2O amounts were obtained from the m/z 44 peak area and instrument N_2O sensitivity⁶⁶.
361 To obtain the conversion factor between peak area and amount of N_2O , the peak areas for
362 reference material amounts from 1 to 40 nmol N_2O were recorded. Standard deviations for
363 inferred N_2O amounts of replicate unknown samples were 0.07 nmol for Lab 1, and 0.19 nmol
364 for Lab 2. All data corrections are described in the README documents associated with
365 pyisotopomer on the Python Package Index⁶⁴.

366

367 **3.3 Lake water unknowns**

368 To validate the scrambling calibration, samples of unknown isotopic composition were
369 collected from Lake Lugano, Switzerland in July 2020 and analyzed separately by both Lab 1
370 and Lab 2. The samples were collected at depths of 10 and 90 meters, including six replicate
371 bottles at each depth. Samples were collected into 160-mL glass serum bottles (Wheaton),
372 overflowing each bottle twice, closing bubble-free, and removing liquid to form a 10-mL
373 headspace comprised of air. Based on the northern hemisphere monthly mean tropospheric N_2O
374 mole fraction when the samples were collected in July, 2020⁷⁰, an atmospheric headspace of this
375 volume would have contained 0.13 nmol N_2O . For Lab 2, where the full amount of N_2O in the
376 sample is measured, incorporation of the headspace into the measurement results in a 0.13 nmol
377 overestimation of the amount of N_2O in the sample. For Lab 1, where 2 mL sample liquid is left
378 behind post-analysis, equilibration the 10-mL headspace during sample storage results in either
379 an underestimate (0.12 nmol) or overestimate (0.10 nmol) of N_2O in the sample, depending on its
380 concentration. In both cases, these errors are similar to the analytical precision of the N_2O
381 amount measurement. Each sample was capped with a gray butyl septum (National Scientific)
382 and sealed with an aluminum crimp seal. Samples were promptly preserved with 100 μL
383 saturated mercuric chloride solution and stored at lab temperature (20-22°C). The isotope effect
384 associated with N_2O partitioning between the gas and liquid phases falls within the analytical
385 uncertainty³³. The six replicate bottles at each depth were split into two groups of three replicate
386 bottles to be measured by Lab 1 and Lab 2, respectively.

387

388 **4. Results and Discussion**

389

390 **4.1 Linearity relation**

391 Linearity relations were calculated using the dummy variable method described in
392 Section 3.2.1 and applied to the intercalibration data as follows. A linearity relation was
393 determined for Lab 1 in February 2021 (Figure 2a-c) and applied to lake water samples run in

394 Lab 1 and reference materials prepared and run in Lab 1. Reference materials prepared in Lab 2
 395 but run in Lab 1 exhibited statistically distinct linearity slopes from those both prepared and run
 396 in Lab 1; thus, a separate linearity relation was applied to these reference materials (but not to the
 397 lake water samples) (Figure 2d-f). A linearity relation was determined for Lab 2 in May 2020
 398 (Figure 2g-i) and applied to lake water samples and reference materials run in Lab 2. As
 399 previously observed⁷¹, for each linearity relation, the slopes of the fits for individual reference
 400 materials were identical within error. The linearity correction reduced the spread of measured
 401 molecular isotope ratios across size series of each given reference material (Figure S2).

402

403 4.2 IRMS scrambling calibration

404 For both labs, the “algebraic” solution produced reasonable values of γ and κ (i.e.,
 405 between 0 and 1) for reference material pairings involving the reference material 53504 ($\delta(^{15}\text{N}^{\text{sp}})$
 406 = -93‰). The mean γ and κ calculated for Lab 1 from reference materials 53504 and CA08214
 407 were 0.174 ± 0.022 and 0.083 ± 0.022 , respectively (Table S2). In August 2020, the mean γ and κ
 408 calculated for Lab 2 from the same two reference materials were 0.095 ± 0.011 and 0.091 ± 0.010 ,
 409 respectively; in November 2020, γ and κ for Lab 2 shifted to 0.091 ± 0.013 and 0.086 ± 0.013 ,
 410 respectively (Table S2). Other reference materials paired with 53504 produced similar values of
 411 γ and κ . The difference $\gamma - \kappa$ was also consistent for reference material pairings with 53504: for
 412 Lab 1, $\gamma - \kappa$ was 0.090-0.091, and for Lab 2, it was 0.003-0.005 (Table S2).

413 For pairings with 53504, the $\delta(^{15}\text{N}^{\text{sp}})$ difference between both reference materials was
 414 greater than 100 ‰. Pairs of reference materials with smaller $\delta(^{15}\text{N}^{\text{sp}})$ differences produced more
 415 variable γ and κ values with the algebraic solution, which sometimes fell outside the physically
 416 plausible range between 0 and 1. For example, in Lab 1, the pairing of CA06261 and CA08214
 417 produced γ and κ values of 0.01 ± 0.23 and -0.08 ± 0.23 , respectively. In this case, the
 418 measurement uncertainty was too large — and the $\delta(^{15}\text{N}^{\text{sp}})$ values too close — for the scrambling
 419 coefficients to be adequately determined. What matters, however, is that the difference between γ
 420 and κ is accurate; as the results show, the absolute values are less important (and can even be
 421 negative, greater than 1, or otherwise “unphysical”).

422 To understand the uncertainty in γ and κ calculated from equations 11 and 12, we define
 423 a variable d :

$$d = \frac{(^{15}\text{R}^\beta + ^{31}\text{R} - ^{45}\text{R})(1 + ^{15}\text{R}^\beta)}{^{15}\text{R}_{\text{atm}}(1 + ^{15}\text{R}^\alpha + ^{15}\text{R}^\beta + ^{31}\text{R} - ^{45}\text{R})} \quad (22)$$

424

425 The value of d is similar for all samples and reference gases run on a given IRMS and
 426 depends primarily on the difference $^{31}\text{R} - ^{45}\text{R}$. Using δ notation, i.e., $\delta(^{15}\text{N}) = ^{15}\text{R}/^{15}\text{R}_{\text{atm}} - 1$, and
 427 dropping the label “ ^{15}N ” for brevity, eqns. (13a) and (13b) can be written as follows:

$$\kappa = \frac{\frac{d_2}{1 + \delta_2^\alpha} - \frac{d_1}{1 + \delta_1^\alpha}}{\frac{1 + \delta_2^\beta}{1 + \delta_2^\alpha} - \frac{1 + \delta_1^\beta}{1 + \delta_1^\alpha}} = \frac{\frac{d_2}{1 + \delta_2^\alpha} - \frac{d_1}{1 + \delta_1^\alpha}}{\frac{\delta_1^{\text{sp}}}{1 + \delta_1^\alpha} - \frac{\delta_2^{\text{sp}}}{1 + \delta_2^\alpha}} \quad (23a)$$

$$\begin{aligned}
\gamma &= \frac{\frac{d_2}{1 + \delta_2^\alpha} \left(\frac{1 + \delta_1^\beta}{1 + \delta_1^\alpha} \right) - \frac{d_1}{1 + \delta_1^\alpha} \left(\frac{1 + \delta_2^\beta}{1 + \delta_2^\alpha} \right)}{\frac{1 + \delta_2^\beta}{1 + \delta_2^\alpha} - \frac{1 + \delta_1^\beta}{1 + \delta_1^\alpha}} \\
&= \frac{\frac{d_2}{1 + \delta_2^\alpha} \left(\frac{1 + \delta_1^\beta}{1 + \delta_1^\alpha} \right) - \frac{d_1}{1 + \delta_1^\alpha} \left(\frac{1 + \delta_2^\beta}{1 + \delta_2^\alpha} \right)}{\frac{\delta_1^{\text{sp}}}{1 + \delta_1^\alpha} - \frac{\delta_2^{\text{sp}}}{1 + \delta_2^\alpha}}
\end{aligned} \tag{23b}$$

428 The denominators of these expressions can be approximated by the difference $\delta_1^{\text{sp}} - \delta_2^{\text{sp}}$.
429 Thus, if the site preferences of the reference gases are similar, the value of the denominator
430 approaches zero and the solutions will become uncertain due to the finite measurement error.
431 Then, the question arises, how far apart must the site preferences of the reference materials be to
432 obtain robust solutions?

433 The general form of uncertainty propagation in a variable a with respect to the
434 observations (y_i) is given by the following equation⁷²:

$$435 \quad \sigma_a^2 = \sum_i \sigma_i^2 \left(\frac{\partial a}{\partial y_i} \right)^2$$

436 where σ_a is the uncertainty in a , y_i is an individual observation, and σ_i is the uncertainty in the
437 observation y_i . Ignoring the uncertainties in ^{45}R and the assigned position-dependent ^{15}R values,
438 the uncertainty in κ can be calculated as:

$$439 \quad \sigma_\kappa^2 = \sigma_{^{31}\text{R}_1}^2 \left(\frac{\partial \kappa}{\partial ^{31}\text{R}_1} \right)^2 + \sigma_{^{31}\text{R}_2}^2 \left(\frac{\partial \kappa}{\partial ^{31}\text{R}_2} \right)^2$$

$$441 \quad \frac{\partial \kappa}{\partial ^{31}\text{R}_1} = \frac{\frac{-(1 + ^{15}\text{R}_1^\alpha)(1 + ^{15}\text{R}_1^\beta)}{^{15}\text{R}_1^\alpha(1 + ^{15}\text{R}_1^\alpha + \text{R}_1^\beta + ^{31}\text{R}_1 - ^{45}\text{R}_1)^2}}{\frac{\delta_1^{\text{sp}}}{1 + \delta_1^\alpha} - \frac{\delta_2^{\text{sp}}}{1 + \delta_2^\alpha}} \approx \frac{-1}{^{15}\text{R}_1^\alpha(\delta_1^{\text{sp}} - \delta_2^{\text{sp}})}$$

$$442 \quad \frac{\partial \kappa}{\partial ^{31}\text{R}_2} = \frac{\frac{-(1 + ^{15}\text{R}_2^\alpha)(1 + ^{15}\text{R}_2^\beta)}{^{15}\text{R}_2^\alpha(1 + ^{15}\text{R}_2^\alpha + \text{R}_2^\beta + ^{31}\text{R}_2 - ^{45}\text{R}_2)^2}}{\frac{\delta_1^{\text{sp}}}{1 + \delta_1^\alpha} - \frac{\delta_2^{\text{sp}}}{1 + \delta_2^\alpha}} \approx \frac{-1}{^{15}\text{R}_2^\alpha(\delta_1^{\text{sp}} - \delta_2^{\text{sp}})}$$

443
444 Assuming $\sigma_{^{31}\text{R}} / ^{15}\text{R}^\alpha = \sigma_{^{31}\text{R}_1} / ^{15}\text{R}_1^\alpha = \sigma_{^{31}\text{R}_2} / ^{15}\text{R}_2^\alpha$, then

$$445 \quad \sigma_\kappa^2 \approx 2 \left(\frac{\sigma_{^{31}\text{R}}}{^{15}\text{R}^\alpha} \right)^2 \left(\frac{1}{\delta_1^{\text{sp}} - \delta_2^{\text{sp}}} \right)^2$$

446 or

$$\sigma_\kappa \approx \sqrt{2} \frac{\sigma(^{31}\text{R})}{^{15}\text{R}^\alpha} \frac{1}{|\delta_1^{\text{sp}} - \delta_2^{\text{sp}}|} \tag{24a}$$

447 Similarly, for γ :

$$\sigma_\gamma \approx \sqrt{2} \frac{\sigma(^{31}R)}{^{15}R^\beta} \frac{1}{|\delta_1^{\text{sp}} - \delta_2^{\text{sp}}|} \quad (24b)$$

448 where $\sigma(^{31}R)/^{15}R$ can be approximated by the measurement uncertainty in $^{31}\delta$ and
 449 $|\delta_1^{\text{sp}} - \delta_2^{\text{sp}}|$ is the absolute value of the difference in assigned site preferences between the two
 450 reference materials. This means that for a measurement uncertainty in $^{31}\delta$ of 1 ‰ and a $\delta(^{15}\text{N}^{\text{sp}})$
 451 difference of 10 ‰ between the two reference materials, γ and κ would have absolute
 452 uncertainties of 0.14. This uncertainty translates into a relative uncertainty of about 30 % for the
 453 $\delta(^{15}\text{N}^{\text{sp}})$ value of an unknown sample – far too high for practical applications (Supplementary
 454 text S4). A $\delta(^{15}\text{N}^{\text{sp}})$ difference of 100 ‰ would give a more useful absolute uncertainty of 0.014
 455 for γ and κ .

456 These theoretical uncertainties are reflected in the experimental data. For Lab 1, the
 457 reference materials 53504 ($\delta(^{15}\text{N}^{\text{sp}}) = -92.73$ ‰) and CA08214 ($\delta(^{15}\text{N}^{\text{sp}}) = 20.54$ ‰) yielded $\gamma =$
 458 0.174 ± 0.022 and $\kappa = 0.083 \pm 0.022$. The standard deviation of $^{31}\delta$ was 1.89 ‰ ($n = 12$). This
 459 produces an estimated uncertainty in γ and κ of $\sqrt{2}(1.89 \text{ ‰})/(113.27 \text{ ‰}) = 0.024$, which agrees
 460 well with the experimental data. Similarly, reference materials 53504 and CA06261 ($\delta(^{15}\text{N}^{\text{sp}}) =$
 461 27.07 ‰) yielded $\gamma = 0.163 \pm 0.018$ and $\kappa = 0.073 \pm 0.018$. The standard deviation of $^{31}\delta$ was 1.58
 462 ‰ ($n = 10$), and the $\delta(^{15}\text{N}^{\text{sp}})$ difference was 119.80 ‰. This produced an estimated uncertainty in
 463 γ and κ of $\sqrt{2}(1.58 \text{ ‰})/(119.80 \text{ ‰}) = 0.019$, also in line with the uncertainties in γ and κ .

464 Rearranging eqns. (24a) and (24b), we obtain expressions for the required $|\delta_1^{\text{sp}} - \delta_2^{\text{sp}}|$ to
 465 obtain a target level of uncertainty (σ) in γ and κ , given the measurement uncertainty in ^{31}R :

$$|\delta_1^{\text{sp}} - \delta_2^{\text{sp}}| = \sqrt{2} \frac{\sigma(^{31}R)}{^{15}R^\alpha} \frac{1}{\sigma_\kappa} \quad (25a)$$

466

$$|\delta_1^{\text{sp}} - \delta_2^{\text{sp}}| = \sqrt{2} \frac{\sigma(^{31}R)}{^{15}R^\beta} \frac{1}{\sigma_\gamma} \quad (25b)$$

467 Assuming $\sigma(^{31}R)/^{15}R^\alpha \approx \sigma(^{31}R)/^{15}R^\beta \approx \sigma(^{31}\delta)$, we obtain:

$$|\delta_1^{\text{sp}} - \delta_2^{\text{sp}}| = \sqrt{2} \sigma(^{31}\delta) \frac{1}{\sigma_{\gamma\kappa}} \quad (26)$$

468

469 where $\sigma(^{31}\delta)$ is the $^{31}\delta$ measurement uncertainty in per mil, and $\sigma_{\gamma\kappa}$ is the target absolute
 470 uncertainty in γ and κ . For example, with a measurement uncertainty of 1 ‰ in $^{31}\delta$, the $\delta(^{15}\text{N}^{\text{sp}})$
 471 values of the two reference materials must differ by at least 141 ‰ to achieve an absolute
 472 uncertainty in γ and κ of 0.01. Based on these results, we recommend calculating γ and κ from
 473 reference materials with a large $\delta(^{15}\text{N}^{\text{sp}})$ difference, as estimated from eqn. (26).

474 As an alternative to the algebraic solution, a least squares optimization can be used to
 475 find a solution for γ and κ , although that solution may find a local optimum rather than a global
 476 optimum. The user can select a least squares optimization instead of the algebraic solution with
 477 the “method” keyword argument to pyisotopomer’s Scrambling function. The least squares
 478 optimization smooths measurement uncertainty, making it useful for fitting repeat

479 measurements of reference materials to a single pair of "best" values for γ and κ . Its disadvantage
 480 is that, unlike the algebraic solution, the least squares optimization depends on the initial guess
 481 for γ and κ . Using data from reference materials CA06261 and CA08214, a range of initial
 482 guesses from $\gamma = \kappa = 0.000$ to $\gamma = \kappa = 0.200$ produced a range of least squares solutions, from $\gamma =$
 483 0.090 and $\kappa = 0.000$ to $\gamma = 0.269$ and $\kappa = 0.183$ (Figure S3). Despite this range of γ and κ ,
 484 however, the least squares optimization produced a consistent $\gamma - \kappa$ of 0.09 . As shown in Section
 485 4.4, $\gamma - \kappa$ governs the accuracy of $\delta(^{15}\text{N}^{\text{sp}})$ far more than the individual values of γ and κ .

486 Given an accurate initial guess, the least squares optimization will find a minimum at or
 487 close to this initial guess, even for reference material pairings close in their $\delta(^{15}\text{N}^{\text{sp}})$. For
 488 example, when we used the algebraic γ and κ from reference materials CA08214 and 53504 as
 489 an initial guess, the least squares optimization produced similar γ and κ for a variety of reference
 490 material pairings (Table S2). Furthermore, for the same initial guess, the least squares
 491 optimization finds different solutions for the Lab 1 and Lab 2 instruments, even for reference
 492 material pairings close in their $\delta(^{15}\text{N}^{\text{sp}})$ (Table S3). This demonstrates that, depending on the
 493 measurement precision at the time, the least squares optimization searches an appropriately wide
 494 solution space to resolve large differences in instrument behavior.

495 If the first-time user wishes to obtain accurate individual values of γ and κ , we
 496 recommend obtaining reference materials different enough in their $\delta(^{15}\text{N}^{\text{sp}})$ to calculate γ and κ
 497 with the algebraic solution. If the user wishes to take advantage of the smoothing of the least
 498 squares optimization, this algebraic γ and κ can then be used as the initial guess for the least
 499 squares solver.

500 We also recommend that the user test the accuracy of the least squares γ and κ by
 501 plugging γ and κ back into eqn. (10) and comparing the result to the measured ^{31}R for each
 502 reference material. The two ^{31}R values should match. pyisotopomer performs this calculation
 503 automatically and outputs the difference as a δ value:

$$^{31}\delta_{\text{error}} = \frac{^{31}\text{R}_{\text{calculated}}}{^{31}\text{R}_{\text{measured}}} - 1 \quad (27)$$

504 where $^{31}\text{R}_{\text{calculated}}$ is calculated by plugging the least squares γ and κ into eqn. (10), and
 505 $^{31}\text{R}_{\text{measured}}$ represents the measured ^{31}R for each reference material. In the intercalibration
 506 exercise, the mean of the absolute values of $^{31}\delta_{\text{error}}$ from least squares γ and κ solutions ranged
 507 from 0.27‰ to 0.86‰ (Table S2), similar in magnitude to the $^{31}\delta$ analytical uncertainty for
 508 Labs 1 and 2 (Table S5). This indicates that the amount of error introduced by using the least
 509 squares optimization is similar to the measurement error in $^{31}\delta$. In comparison, the $^{31}\delta_{\text{error}}$
 510 introduced by the algebraic solution corresponded to values of $(^{31}\text{R}_{\text{calculated}} - ^{31}\text{R}_{\text{measured}})$ within
 511 machine precision (Table S2).

514 4.3 Variability in fragmentation behavior

515 As shown above, $\gamma - \kappa$, as opposed to the individual values of γ and κ , is the best
 516 constrained parameter in the scrambling calculation. We show below that $\gamma - \kappa$ also has the
 517 greatest impact on $\delta(^{15}\text{N}^{\text{a}})$, $\delta(^{15}\text{N}^{\text{b}})$, and $\delta(^{15}\text{N}^{\text{sp}})$. $\gamma - \kappa$ is proportional to $^{31}\delta - ^{45}\delta$, and thus is a
 518 metric of an instrument's scrambling behavior.

519 To examine the change in the fragmentation behavior of a single IRMS over time, we
 520 compiled values of $\gamma - \kappa$ for Lab 1 from June 2018 – March 2021 (Figure 3). To equally weigh

521 each day of running the instrument, first, we calculated a daily mean $\gamma - \kappa$, then calculated a five-
 522 day running average of $\gamma - \kappa$ from these daily means. The value of $\gamma - \kappa$ varied throughout the
 523 time series, with a mean of 0.092 ± 0.002 . High volatility in $\gamma - \kappa$ in February-April 2019
 524 corresponded with a period when the lab temperature was poorly controlled, with strong day-
 525 night variation (Figure 3). During periods when the lab temperature was stable, $\gamma - \kappa$ tended to
 526 increase as the instrument box and trap currents diverged with filament age, although no linear
 527 relationship emerged

528 There are several reasons why the scrambling behavior of the ion source might change
 529 over time. The NO^+ fragment ion can be produced by one of several routes from N_2O^+ ^{73,74}. The
 530 pathways and associated isotope effects for the formation of fragment ions are affected by
 531 collision frequency, the distribution of excited states, and the time spent in the ion source, which
 532 suggests that ion source conditions such as vapor pressure, ionizing energy, and accelerating
 533 voltage may all influence the fragmentation behavior of an IRMS system^{54,73-76}. For these
 534 reasons, performing the scrambling calibration only once is insufficient to obtain high-quality
 535 N_2O isotopocule data. Instead, it is important to recalibrate an IRMS system for scrambling on a
 536 regular basis since ion source conditions may change with time and can shift abruptly with
 537 events such as filament changes. We recommend using a running average of γ and κ over a
 538 window corresponding to 10 pairings of reference materials, corresponding to a five-day window
 539 if two pairs of reference materials are run per day. If there is high volatility in γ and κ , as seen
 540 above in March-April 2019, it may be necessary to shorten this window, to apply scrambling
 541 corrections most appropriate to instrument conditions.

543 4.4 Sensitivity of position-dependent δ values to uncertainty in scrambling coefficients

544 The uncertainty in $\delta(^{15}\text{N}^\alpha)$, $\delta(^{15}\text{N}^\beta)$, and $\delta(^{15}\text{N}^{\text{sp}})$ associated with the uncertainty in each
 545 scrambling coefficient is less straightforward to assess than the uncertainty in ^{31}R given by eqns.
 546 (23) and (24), due to the nonlinear relationship between $\delta(^{15}\text{N}^\alpha)$, $\delta(^{15}\text{N}^\beta)$, γ , and κ . (see eqn. (53)
 547 of Kaiser and Röckmann, 2008). A first order approximation of $\delta(^{15}\text{N}^{\text{sp}})$ is given by
 548 (supplementary text S4):

$$\delta(^{15}\text{N}^{\text{sp}}) \approx \frac{2(1 - \gamma + \kappa)}{1 - \gamma - \kappa} ({}^{31}\delta - {}^{45}\delta) \quad (28)$$

549 From this equation, it is apparent that $\delta(^{15}\text{N}^{\text{sp}})$ is modulated primarily by the difference γ
 550 $- \kappa$, rather than the individual values of γ and κ . It is also apparent that $\gamma - \kappa$ is proportional to ${}^{31}\delta$
 551 $- {}^{45}\delta$.

552 A Monte Carlo simulation can be a useful way of visualizing how γ , κ , and, $\gamma - \kappa$ impact
 553 $\delta(^{15}\text{N}^\alpha)$, $\delta(^{15}\text{N}^\beta)$, and $\delta(^{15}\text{N}^{\text{sp}})$. We performed two sensitivity experiments with data from Lab 1:

- 554 1) sensitivity of $\delta(^{15}\text{N}^\alpha)$, $\delta(^{15}\text{N}^\beta)$, and $\delta(^{15}\text{N}^{\text{sp}})$ to $\gamma - \kappa$;
- 555 2) sensitivity of $\delta(^{15}\text{N}^\alpha)$, $\delta(^{15}\text{N}^\beta)$, and $\delta(^{15}\text{N}^{\text{sp}})$ to the individual values of γ and κ , holding
 556 their difference constant.

557 For the first sensitivity experiment, a Monte Carlo simulation was used to introduce
 558 random uncertainty in the γ and κ values used to calculate δ values of three reference materials.
 559 Based Table S2, we chose $\gamma = 0.174$ and $\kappa = 0.083$ as central values and varied $\gamma - \kappa$ such that
 560 the standard deviation of $\gamma - \kappa$ was equal to 10 % of the mean (0.091). For the second sensitivity
 561 experiment, we modeled γ and κ in tandem as random numbers centered around $\gamma = 0.174$ and κ
 562 $= 0.083$, with uncertainties equal to 10 % of the mean γ , and held $\gamma - \kappa$ constant at 0.091. For
 563 both experiments, we sampled 1000 pairs of γ and κ , and then calculated the 1000 simulated

564 values of $\delta(^{15}\text{N}^\alpha)$, $\delta(^{15}\text{N}^\beta)$, and $\delta(^{15}\text{N}^{\text{sp}})$ for the three reference materials (CA06261, 53504,
565 CA08214).

566 This analysis showed that a 10 % relative uncertainty in $\gamma - \kappa$ can lead to large variations
567 in $\delta(^{15}\text{N}^\alpha)$, $\delta(^{15}\text{N}^\beta)$, and $\delta(^{15}\text{N}^{\text{sp}})$, e.g., pooled standard deviations of 17.1-18.5 ‰ for $\delta(^{15}\text{N}^{\text{sp}})$
568 (Figure 4a-c). In contrast, a 10 % relative error in γ , keeping $\gamma - \kappa$ constant, led to pooled
569 standard deviations of 1.0-4.3 ‰ in $\delta(^{15}\text{N}^{\text{sp}})$ (Figure 4d-f). In both experiments, varying γ and κ
570 produced the most variability for reference material 53504, whose $\delta(^{15}\text{N}^{\text{sp}})$ was greatest in
571 magnitude.

572 These results reflect the earlier conclusion that $\gamma - \kappa$ is the best constrained parameter in
573 the scrambling calculation, and, conversely, that this difference has the greatest effect on
574 $\delta(^{15}\text{N}^{\text{sp}})$. Thus, we recommend regular scrambling calibrations, as assuming the wrong $\gamma - \kappa$
575 difference may have a significant impact on site preferences calculated from these coefficients.
576

577 **4.5 Comparison of results between two IRMS laboratories**

578 The application of pyisotopomer was tested through an intercalibration including four
579 reference materials and two Lake Lugano samples measured by two IRMS laboratories, plus two
580 additional reference materials run in Lab 1. Using an average γ and κ produced by the algebraic
581 method from the pairing of reference materials 53504 and CA08214, isotopomers were
582 calculated for lake water unknowns, four reference materials run as unknowns for quality
583 control, and the two reference materials used in the calibration and (Table 2). This exercise was
584 repeated, calculating γ and κ instead with least squares method and the pairing of reference
585 materials CA06261 and CA08214 (Table S4). The root mean square deviation (RMSD) for each
586 reference material was calculated by comparison to the calibrated values provided by a previous
587 intercalibration effort⁵⁶ (for atmosphere-equilibrated seawater), an internal standard (B6), and for
588 gases sourced from J. Mohn (S2, CA06261, 53504, and CA08214). Almost all isotopomer values
589 produced by the least squares optimization (Table S4) were within error of those produced by the
590 algebraic solution (Table 2); the latter is discussed below.

591 The $\delta(^{15}\text{N}^{\text{bulk}})$ measured by the two labs displayed good agreement for each of the four
592 reference materials, as well as the lake water samples. The $\delta(^{15}\text{N}^{\text{bulk}})$ RMSDs ranged from 0.2 to
593 0.6 ‰ (Table 2), all of which were smaller than the 0.8 ‰ presented for IRMS labs by Mohn et
594 al., (2014). The RMSD for atmospheric N_2O was highest, at 0.6 ‰. For both lake water samples,
595 the $\delta(^{15}\text{N}^{\text{bulk}})$ values measured by Lab 1 and Lab 2 were statistically indistinguishable (Table 2;
596 Figure S4). Likewise, the $\delta(^{18}\text{O})$ measured by the two labs displayed good agreement for each of
597 the four reference materials measured by both labs, as well as the lake water samples. The $\delta(^{18}\text{O})$
598 RMSDs were slightly greater than the 1.00 ‰ presented for IRMS labs by Mohn et al. (2014),
599 ranging from 0.5 ‰–1.7 ‰, with the greatest RMSD for reference material 53504 (Table 2). For
600 the lake water unknowns, the $\delta(^{18}\text{O})$ values measured by the two labs were within error of each
601 other (Table 2; Figure S4).

602 The $\delta(^{15}\text{N}^\alpha)$ measured by the two labs also showed good agreement for reference
603 materials CA06261, CA08214, and atmosphere-equilibrated seawater: in each case, the
604 combined RMSD was less than 2.4 ‰ (Table 2). This is similar to the data presented in Mohn et
605 al. (2014), who find an RMSD for $\delta(^{15}\text{N}^\alpha)$ for IRMS laboratories of 2.47 ‰. The $\delta(^{15}\text{N}^\alpha)$
606 measured by Lab 1 for reference material 53504 (0.0 ± 1.0 ‰) was lower than both the calibrated
607 value (1.71 ‰) and the value measured by Lab 2 (1.7 ± 1.0 ‰). The values of $\delta(^{15}\text{N}^\alpha)$ measured
608 by the two labs for the two lake water samples, however, were within error of each other. For
609 $\delta(^{15}\text{N}^\beta)$, the RMSDs for each reference material were of a similar order of magnitude to $\delta(^{15}\text{N}^\alpha)$,

610 ranging from 0.2 ‰-2.1 ‰, similar to the value 2.12 ‰ reported by Mohn et al. (2014). The
611 $\delta(^{15}\text{N}^\beta)$ measured by Lab 1 for the lake water unknowns was within error of that measured by
612 Lab 2 (Table 2; Figure S4). Of note, the $\delta(^{15}\text{N}^\beta)$ for the lake water unknown taken at 90 m depth
613 was -32.8 ‰ (average of measurements by Lab 1 and Lab 2), which is far more negative than
614 most values observed previously^{26,31}.

615 The $\delta(^{15}\text{N}^{\text{sp}})$ values measured by the two laboratories showed larger standard deviations
616 than the $\delta(^{15}\text{N}^\alpha)$ and $\delta(^{15}\text{N}^\beta)$ individually, which is to be expected, since $\delta(^{15}\text{N}^{\text{sp}})$ is a measure of
617 difference between the latter two parameters. The $\delta(^{15}\text{N}^{\text{sp}})$ RMSD values, however, were all less
618 than 3 ‰ for atmosphere-equilibrated seawater, 53504, and CA08214 (Table 2). This represents
619 an improvement on Mohn et al. (2014), who find an RMSD of 4.29 ‰ for $\delta(^{15}\text{N}^{\text{sp}})$ measured by
620 IRMS laboratories. The $\delta(^{15}\text{N}^{\text{sp}})$ RMSD for reference material CA06261 was greater, at 4.4 ‰,
621 which may result from this reference material having a more negative $\delta(^{15}\text{N}^\alpha)$ than either of the
622 two reference materials used in the scrambling calibration. The lake water samples showed larger
623 offsets in $\delta(^{15}\text{N}^{\text{sp}})$ than the reference materials (Figure S4). The lake water sample from 10 m
624 depth showed an especially large difference in $\delta(^{15}\text{N}^{\text{sp}})$ between Lab 1 and Lab 2: Lab 1
625 measured a mean $\delta(^{15}\text{N}^{\text{sp}})$ of (18.8 ± 1.6) ‰ at this depth, while Lab 2 measured a mean $\delta(^{15}\text{N}^{\text{sp}})$
626 of (21.4 ± 2.5) ‰ (Table 2). At 90 m depth, Lab 1 measured a mean $\delta(^{15}\text{N}^{\text{sp}})$ of 52.3 ± 1.2 ‰, and
627 Lab 2 measured a mean $\delta(^{15}\text{N}^{\text{sp}})$ of (50.9 ± 0.5) ‰.

628 After size correction and scale normalization, the only consistent difference between
629 measurements made by the two labs were differences in peak area, which may reflect differences
630 in the setup of the purge and trap system and/or differences in instrument sensitivity. The N_2O
631 amounts measured in the lake water samples, however, were also similar between the two labs
632 involved in the intercalibration exercise, indicating that this difference in sensitivity was
633 adequately compensated for by the peak area to amount conversion factor. In the sample taken at
634 10 m depth, Lab 1 found (2.97 ± 0.04) nmol; Lab 2 found (2.31 ± 0.09) nmol. At 90 m depth, Lab 1
635 found (20.46 ± 0.37) nmol; Lab 2 found (19.82 ± 0.01) nmol N_2O . All bottle volumes were the
636 same. Thus, we conclude that differences in sample pretreatment procedure were corrected for
637 by the size correction and scale normalization steps, leaving no residual effect on the final δ
638 values or N_2O amounts.

639

640 4.6 Additional considerations

641 The pyisotopomer package produces good results if each of the data preprocessing steps
642 properly account for size- and delta-dependent effects on the measured isotope ratios $^{31}\delta$, $^{45}\delta$, and
643 $^{46}\delta$. However, it will produce spurious results under the following circumstances. Firstly, varying
644 blanks may introduce errors due to the size correction not being applicable to samples and
645 reference materials alike. Second, if the $^{45}\delta$ and $^{46}\delta$ scale normalization slope and intercept differ
646 substantially from one and zero (such as a negative slope), there likely exists an issue with the
647 scale normalization (such as the reference materials not spanning a wide enough range in $^{45}\delta$ and
648 $^{46}\delta$). A spurious scale normalization will likewise produce errors in the final isotopocule values.
649 Thirdly, if reference materials that are too close in their site preferences are used to determine γ
650 and κ with the algebraic solution, the resulting coefficients may represent "unphysical" values
651 (i.e., not between 0 and 1); these, however, would be inconsequential if the unknown samples
652 have $\delta(^{15}\text{N}^{\text{sp}})$ values close to these reference materials. Finally, $\delta(^{17}\text{O})$ is calculated from a mass
653 dependent relationship with $\delta(^{18}\text{O})$ (the parameters of which can be adjusted with keyword
654 arguments to the Scrambling and Isotopomers functions) unless $\Delta(^{17}\text{O})$ is determined
655 separately^{59,61,62} and entered in the data corrections template.

656

657 **5. Conclusion: How to obtain high-quality N₂O isotopocule data using pyisotopomer**

658 Using pyisotopomer and three reference materials, one can characterize the scrambling
659 behavior for a given IRMS and apply those scrambling coefficients to calculate the isotopocule
660 values of unknown samples. To ensure high-quality results from these calculations, we provide
661 the following recommendations. Firstly, if reference materials with suitably distinct site
662 preferences are available, we recommend calculating the scrambling coefficients γ and κ from
663 algebraic solution of eqns. (11) and (12), which is the default method in the Scrambling function
664 of pyisotopomer. We offer the least squares approach as an alternative, with the following
665 caveats: 1) The least squares solver finds a minimum close to the initial guess for γ and κ . As
666 such, if the solver is fed an initial guess other than the absolute minimum calculated from the
667 algebraic solution, it will find the “wrong” absolute value of γ and κ . It will, however, find the
668 correct value of $\gamma - \kappa$, which has a much larger impact on calculated isotopocules. 2) Using the
669 “wrong” scrambling coefficients will have only a small effect if the unknowns are close in their
670 $\delta(^{15}\text{N}^\alpha)$, $\delta(^{15}\text{N}^\beta)$, and $\delta(^{15}\text{N}^{\text{sp}})$ to those of the reference materials but will have a deleterious effect
671 as the unknowns diverge in their isotopomer values from the reference materials. 3) If an initial
672 guess is available, such as through a calibration with the algebraic solution, this should be used
673 as the initial guess for the least squares solver. Otherwise, we recommend iterating through the
674 scrambling calculation twice. Use the solution from the first iteration as the initial guess for
675 subsequent calculations. 4) It is necessary to run paired reference materials daily to obtain
676 accurate running estimates of γ and κ . It is recommended to convert these daily estimates to a
677 one-week running average and use that average to calculate the isotopocules of unknown
678 samples.

679 Using pyisotopomer in an intercalibration exercise and implementing the above
680 recommendations, we find good agreement between the calibrated δ values measured by two
681 different IRMS labs for both reference materials and natural lake samples. We conclude that
682 while the intercalibration results demonstrate potential for further improvement in precision, the
683 intercalibration of $\delta(^{15}\text{N}^{\text{sp}})$ using a uniform scrambling calculation (pyisotopomer) presented here
684 represents an improvement upon previous N₂O intercalibrations.

685

686 **Data availability statement**

687 The manuscript is prepared to comply with the RCMS data policy. The latest version of
688 pyisotopomer is available for installation via the Python Package index
689 (pypi.org/project/pyisotopomer). The second release of pyisotopomer is also available via
690 Zenodo (doi.org/10.5281/zenodo.7552724). This research was supported by U.S.-NSF grant
691 OCE-1657868 to K. L. Casciotti. C. L. Kelly is supported by an NSF Graduate Research
692 Fellowship. The authors declare no competing financial interests.

693 **References**

694

695 1. Yung YL, Wang WC, Lacis AA. Greenhouse effect due to atmospheric nitrous oxide.
696 *Geophys Res Lett.* 1976;3(10):619-621. doi:10.1029/GL003i010p00619

697 2. Smith C, Nicholls ZRJ, Armour K, et al. The Earth's Energy Budget, Climate Feedbacks,
698 and Climate Sensitivity Supplementary Material. In: Masson-Delmotte V, Zhai P, Pirani A,
699 et al., eds. *Climate Change 2021: The Physical Science Basis. Contribution of Working*
700 *Group I to the Sixth Assessment Report of the Intergovernmental Panel on Climate Change.*
701 Cambridge University Press; 2021. Accessed October 4, 2021.
702 https://www.ipcc.ch/report/ar6/wg1/downloads/report/IPCC_AR6_WGI_Chapter_07_Supplementary_Material.pdf
703

704 3. Crutzen PJ. The influence of nitrogen oxides on the atmospheric ozone content. *Q J R*
705 *Meteorol Soc.* 1970;96(408):320-325. doi:10.1002/qj.49709640815

706 4. Ravishankara AR, Daniel JS, Portmann RW. Nitrous Oxide (N₂O): The Dominant Ozone-
707 Depleting Substance Emitted in the 21st Century. *Science.* 2009;326(5949):123-125.
708 doi:10.1126/science.1176985

709 5. Wuebbles DJ. Nitrous Oxide: No Laughing Matter. *Science.* 2009;326(5949):56-57.
710 doi:10.1126/science.1179571

711 6. Müller R. The impact of the rise in atmospheric nitrous oxide on stratospheric ozone.
712 *Ambio.* 2021;50(1):35-39. doi:10.1007/s13280-020-01428-3

713 7. Kim KR, Craig H. Nitrogen-15 and Oxygen-18 Characteristics of Nitrous Oxide: A Global
714 Perspective. *Science.* 1993;262(5141):1855-1857. doi:10.1126/science.262.5141.1855

715 8. Pérez T, Trumbore SE, Tyler SC, Davidson EA, Keller M, Camargo PB de. Isotopic
716 variability of N₂O emissions from tropical forest soils. *Glob Biogeochem Cycles.*
717 2000;14(2):525-535. doi:10.1029/1999GB001181

718 9. Kim KR, Craig H. Two-isotope characterization of N₂O in the Pacific Ocean and
719 constraints on its origin in deep water. *Nature.* 1990;347(6288):58-61.
720 doi:10.1038/347058a0

721 10. Dore JE, Popp BN, Karl DM, Sansone FJ. A large source of atmospheric nitrous oxide from
722 subtropical North Pacific surface waters. *Nature.* 1998;396(6706):63-66.
723 doi:10.1038/23921

724 11. Naqvi SWA, Naik H, Jayakumar A, et al. Seasonal Anoxia Over the Western Indian
725 Continental Shelf. In: Wiggert JD, Hood RR, Naqvi SWA, Brink KH, Smith SL, eds.
726 *Geophysical Monograph Series.* Vol 185. American Geophysical Union; 2009:333-345.
727 doi:10.1029/2008GM000745

728 12. Yoshida N, Hattori A, Saino T, Matsuo S, Wada E. 15N/14N ratio of dissolved N₂O in the
729 eastern tropical Pacific Ocean. *Nature.* Published online 1984. doi:10.1038/307442A0

- 730 13. Rahn T, Wahlen M. Stable Isotope Enrichment in Stratospheric Nitrous Oxide. *Science*.
731 1997;278(5344):1776-1778. doi:10.1126/science.278.5344.1776
- 732 14. Rahn T, Wahlen M. A reassessment of the global isotopic budget of atmospheric nitrous
733 oxide. *Glob Biogeochem Cycles*. 2000;14(2):537-543. doi:10.1029/1999GB900070
- 734 15. Yoshida N. ¹⁵N-depleted N₂O as a product of nitrification. *Nature*. 1988;335(6190):528-
735 529. doi:10.1038/335528a0
- 736 16. Barford CC, Montoya JP, Altabet MA, Mitchell R. Steady-State Nitrogen Isotope Effects of
737 N₂ and N₂O Production in *Paracoccus denitrificans*. *Appl Environ Microbiol*.
738 1999;65(3):989-994. doi:10.1128/AEM.65.3.989-994.1999
- 739 17. Pérez T, Trumbore SE, Tyler SC, et al. Identifying the agricultural imprint on the global
740 N₂O budget using stable isotopes. *J Geophys Res Atmospheres*. 2001;106(D9):9869-9878.
741 doi:10.1029/2000JD900809
- 742 18. Yamulki S, Toyoda S, Yoshida N, Veldkamp E, Grant B, Bol R. Diurnal fluxes and the
743 isotopomer ratios of N₂O in a temperate grassland following urine amendment. *Rapid*
744 *Commun Mass Spectrom*. 2001;15(15):1263-1269. doi:10.1002/rcm.352
- 745 19. Lewicka-Szczebak D, Augustin J, Gieseemann A, Well R. Quantifying N₂O reduction to N₂
746 based on N₂O isotopocules – validation with independent methods (helium incubation and
747 ¹⁵N gas flux method). *Biogeosciences*. 2017;14(3):711-732. doi:https://doi.org/10.5194/bg-
748 14-711-2017
- 749 20. Verhoeven E, Barthel M, Yu L, et al. Early season N₂O emissions under variable water
750 management in rice systems: source-partitioning emissions using isotope ratios along a
751 depth profile. *Biogeosciences*. 2019;16(2):383-408. doi:https://doi.org/10.5194/bg-16-383-
752 2019
- 753 21. Yoshida N, Toyoda S. Constraining the atmospheric N₂O budget from intramolecular site
754 preference in N₂O isotopomers. *Nature*. 2000;405(6784):330-334. doi:10.1038/35012558
- 755 22. Prokopiou M, Martinerie P, Link to external site this link will open in a new window, et al.
756 Constraining N₂O emissions since 1940 using firm air isotope measurements in both
757 hemispheres. *Atmospheric Chem Phys*. 2017;17(7):4539-4564. doi:10.5194/acp-17-4539-
758 2017
- 759 23. Yu L, Harris E, Henne S, et al. The isotopic composition of atmospheric nitrous oxide
760 observed at the high-altitude research station Jungfraujoch, Switzerland. *Atmospheric Chem*
761 *Phys*. 2020;20(11):6495-6519. doi:10.5194/acp-20-6495-2020
- 762 24. Toyoda S, Yoshida N, Miwa T, et al. Production mechanism and global budget of N₂O
763 inferred from its isotopomers in the western North Pacific. *Geophys Res Lett*. 2002;29(3):7-
764 1-7-4. doi:10.1029/2001GL014311

- 765 25. Popp BN, Westley MB, Toyoda S, et al. Nitrogen and oxygen isotopomeric constraints on
766 the origins and sea-to-air flux of N₂O in the oligotrophic subtropical North Pacific gyre.
767 *Glob Biogeochem Cycles*. 2002;16(4):12-1-12-10. doi:10.1029/2001GB001806
- 768 26. Yamagishi H, Westley MB, Popp BN, et al. Role of nitrification and denitrification on the
769 nitrous oxide cycle in the eastern tropical North Pacific and Gulf of California. *J Geophys*
770 *Res Biogeosciences*. 2007;112(G2). doi:10.1029/2006JG000227
- 771 27. Yamagishi H, Yoshida N, Toyoda S, Popp BN, Westley MB, Watanabe S. Contributions of
772 denitrification and mixing on the distribution of nitrous oxide in the North Pacific. *Geophys*
773 *Res Lett*. 2005;32(4). doi:10.1029/2004GL021458
- 774 28. Westley MB, Yamagishi H, Popp BN, Yoshida N. Nitrous oxide cycling in the Black Sea
775 inferred from stable isotope and isotopomer distributions. *Deep Sea Res Part II Top Stud*
776 *Oceanogr*. 2006;53(17-19):1802-1816. doi:10.1016/j.dsr2.2006.03.012
- 777 29. Farías L, Castro-González M, Cornejo M, et al. Denitrification and nitrous oxide cycling
778 within the upper oxycline of the eastern tropical South Pacific oxygen minimum zone.
779 *Limnol Oceanogr*. 2009;54(1):132-144. doi:10.4319/lo.2009.54.1.0132
- 780 30. Casciotti KL, Forbes M, Vedamati J, Peters BD, Martin TS, Mordy CW. Nitrous oxide
781 cycling in the Eastern Tropical South Pacific as inferred from isotopic and isotopomeric
782 data. *Deep Sea Res Part II Top Stud Oceanogr*. 2018;156:155-167.
783 doi:10.1016/j.dsr2.2018.07.014
- 784 31. Bourbonnais A, Letscher RT, Bange HW, et al. N₂O production and consumption from
785 stable isotopic and concentration data in the Peruvian coastal upwelling system. *Glob*
786 *Biogeochem Cycles*. 2017;31(4):678-698. doi:10.1002/2016GB005567
- 787 32. Toyoda S, Yoshida O, Yamagishi H, Fujii A, Yoshida N, Watanabe S. Identifying the
788 origin of nitrous oxide dissolved in deep ocean by concentration and isotopocule analyses.
789 *Sci Rep*. 2019;9(1):1-9. doi:10.1038/s41598-019-44224-0
- 790 33. Kelly CL, Travis NM, Baya PA, Casciotti KL. Quantifying Nitrous Oxide Cycling Regimes
791 in the Eastern Tropical North Pacific Ocean With Isotopomer Analysis. *Glob Biogeochem*
792 *Cycles*. 2021;35(2):e2020GB006637. doi:10.1029/2020GB006637
- 793 34. Toyoda S, Kakimoto T, Kudo K, et al. Distribution and Production Mechanisms of N₂O in
794 the Western Arctic Ocean. *Glob Biogeochem Cycles*. 2021;35(4):e2020GB006881.
795 doi:https://doi.org/10.1029/2020GB006881
- 796 35. Friedman L, Bigeleisen J. Oxygen and Nitrogen Isotope Effects in the Decomposition of
797 Ammonium Nitrate. *J Chem Phys*. 1950;18(10):1325-1331. doi:10.1063/1.1747471
- 798 36. Toyoda S, Yoshida N. Determination of nitrogen isotopomers of nitrous oxide on a
799 modified isotope ratio mass spectrometer. *Anal Chem*. 1999;71(20):4711-4718.
800 doi:10.1021/ac9904563

- 801 37. Brenninkmeijer CAM, Röckmann T. Mass spectrometry of the intramolecular nitrogen
802 isotope distribution of environmental nitrous oxide using fragment-ion analysis. *Rapid*
803 *Commun Mass Spectrom.* 1999;13(20):2028-2033. doi:10.1002/(SICI)1097-
804 0231(19991030)13:20<2028::AID-RCM751>3.0.CO;2-J
- 805 38. Kaiser J, Brenninkmeijer CAM, Röckmann T. Intramolecular ¹⁵N and ¹⁸O fractionation in
806 the reaction of N₂O with O(¹D) and its implications for the stratospheric N₂O isotope
807 signature. *J Geophys Res Atmospheres.* 2002;107(D14):ACH 16-1-ACH 16-14.
808 doi:10.1029/2001JD001506
- 809 39. Kaiser J. *Stable Isotope Investigations of Atmospheric Nitrous Oxide.* Johannes Gutenberg
810 University of Mainz; 2003. <https://doi.org/10.25358/openscience-3976>
- 811 40. Röckmann T, Levin I. High-precision determination of the changing isotopic composition
812 of atmospheric N₂O from 1990 to 2002. *J Geophys Res Atmospheres.* 2005;110(D21).
813 doi:10.1029/2005JD006066
- 814 41. Yung YL, Miller CE. Isotopic Fractionation of Stratospheric Nitrous Oxide. *Science.*
815 1997;278(5344):1778-1780. doi:10.1126/science.278.5344.1778
- 816 42. Röckmann T, Kaiser J, Brenninkmeijer CAM, et al. Isotopic enrichment of nitrous oxide
817 (¹⁵N¹⁴NO, ¹⁴N¹⁵NO, ¹⁴N¹⁴N¹⁸O) in the stratosphere and in the laboratory. *J Geophys*
818 *Res Atmospheres.* 2001;106(D10):10403-10410. doi:10.1029/2000JD900822
- 819 43. Toyoda S, Yoshida N, Urabe T, et al. Temporal and latitudinal distributions of stratospheric
820 N₂O isotopomers. *J Geophys Res Atmospheres.* 2004;109(D8). doi:10.1029/2003JD004316
- 821 44. Kaiser J, Engel A, Borchers R, Rockmann T. Probing stratospheric transport and chemistry
822 with new balloon and aircraft observations of the meridional and vertical N₂O isotope
823 distribution. *Atmos Chem Phys.* Published online 2006:22.
- 824 45. Park S, Atlas EL, Boering KA. Measurements of N₂O isotopologues in the stratosphere:
825 Influence of transport on the apparent enrichment factors and the isotopologue fluxes to the
826 troposphere. *J Geophys Res Atmospheres.* 2004;109(D1). doi:10.1029/2003JD003731
- 827 46. Sutka RL, Ostrom NE, Ostrom PH, Gandhi H, Breznak JA. Nitrogen isotopomer site
828 preference of N₂O produced by *Nitrosomonas europaea* and *Methylococcus capsulatus*
829 Bath. *Rapid Commun Mass Spectrom RCM.* 2003;17(7):738-745. doi:10.1002/rcm.968
- 830 47. Sutka RL, Ostrom NE, Ostrom PH, et al. Distinguishing Nitrous Oxide Production from
831 Nitrification and Denitrification on the Basis of Isotopomer Abundances. *Appl Environ*
832 *Microbiol.* 2006;72(1):638-644. doi:10.1128/AEM.72.1.638-644.2006
- 833 48. Sutka RL, Ostrom NE, Ostrom PH, Gandhi H, Breznak JA. Nitrogen isotopomer site
834 preference of N₂O produced by *Nitrosomonas europaea* and *Methylococcus capsulatus*
835 Bath. *Rapid Commun Mass Spectrom.* 2004;18(12):1411-1412. doi:10.1002/rcm.1482

- 836 49. Toyoda S, Mutobe H, Yamagishi H, Yoshida N, Tanji Y. Fractionation of N₂O isotopomers
837 during production by denitrifier. *Soil Biol Biochem.* 2005;37(8):1535-1545.
838 doi:10.1016/j.soilbio.2005.01.009
- 839 50. Frame CH, Casciotti KL. Biogeochemical controls and isotopic signatures of nitrous oxide
840 production by a marine ammonia-oxidizing bacterium. *Biogeosciences.* 2010;7(9):2695-
841 2709. doi:10.5194/bg-7-2695-2010
- 842 51. Schmidt HL, Werner RA, Yoshida N, Well R. Is the isotopic composition of nitrous oxide
843 an indicator for its origin from nitrification or denitrification? A theoretical approach from
844 referred data and microbiological and enzyme kinetic aspects. *Rapid Commun Mass*
845 *Spectrom.* 2004;18(18):2036-2040. doi:10.1002/rcm.1586
- 846 52. Ostrom NE, Pitt A, Sutka R, et al. Isotopologue effects during N₂O reduction in soils and in
847 pure cultures of denitrifiers. *J Geophys Res Biogeosciences.* 2007;112(G2).
848 doi:10.1029/2006JG000287
- 849 53. Kaiser J, Park S, Boering KA, Brenninkmeijer CAM, Hilker A, Röckmann T. Mass
850 spectrometric method for the absolute calibration of the intramolecular nitrogen isotope
851 distribution in nitrous oxide. *Anal Bioanal Chem.* 2004;378(2):256-269.
852 doi:10.1007/s00216-003-2233-2
- 853 54. Westley MB, Popp BN, Rust TM. The calibration of the intramolecular nitrogen isotope
854 distribution in nitrous oxide measured by isotope ratio mass spectrometry. *Rapid Commun*
855 *Mass Spectrom.* 2007;21(3):391-405. doi:10.1002/rcm.2828
- 856 55. Ostrom NE, Gandhi H, Coplen TB, et al. Preliminary assessment of stable nitrogen and
857 oxygen isotopic composition of USGS51 and USGS52 nitrous oxide reference gases and
858 perspectives on calibration needs. *Rapid Commun Mass Spectrom.* 2018;32(15):1207-1214.
859 doi:10.1002/rcm.8157
- 860 56. Mohn J, Wolf B, Toyoda S, et al. Interlaboratory assessment of nitrous oxide isotopomer
861 analysis by isotope ratio mass spectrometry and laser spectroscopy: current status and
862 perspectives. *Rapid Commun Mass Spectrom.* 2014;28(18):1995-2007.
863 doi:10.1002/rcm.6982
- 864 57. Baertschi P. Absolute ¹⁸O content of standard mean ocean water. *Earth Planet Sci Lett.*
865 1976;31(3):341-344. doi:10.1016/0012-821X(76)90115-1
- 866 58. Jabeen I, Kusakabe M. Determination of δ ¹⁷O values of reference water samples VSMOW
867 and SLAP. *Chem Geol.* 1997;143:115-119. doi:10.1016/S0009-2541(97)00109-5
- 868 59. Kaiser J, Röckmann T, Brenninkmeijer CAM. Complete and accurate mass spectrometric
869 isotope analysis of tropospheric nitrous oxide. *J Geophys Res Atmospheres.*
870 2003;108(D15). doi:10.1029/2003JD003613

- 871 60. Kaiser J, Röckmann T. Correction of mass spectrometric isotope ratio measurements for
872 isobaric isotopologues of O₂, CO, CO₂, N₂O and SO₂. *Rapid Commun Mass Spectrom.*
873 2008;22(24):3997-4008. doi:10.1002/rcm.3821
- 874 61. Kaiser J, Hastings MG, Houlton BZ, Röckmann T, Sigman DM. Triple Oxygen Isotope
875 Analysis of Nitrate Using the Denitrifier Method and Thermal Decomposition of N₂O.
876 *Anal Chem.* 2007;79(2):599-607. doi:10.1021/ac061022s
- 877 62. Wankel SD, Ziebis W, Buchwald C, et al. Evidence for fungal and chemodenitrification
878 based N₂O flux from nitrogen impacted coastal sediments. *Nat Commun.* 2017;8(1):1-11.
879 doi:10.1038/ncomms15595
- 880 63. Magyar PM, Orphan VJ, Eiler JM. Measurement of rare isotopologues of nitrous oxide by
881 high-resolution multi-collector mass spectrometry. *Rapid Commun Mass Spectrom.*
882 2016;30(17):1923-1940. doi:10.1002/rcm.7671
- 883 64. Kelly CL. ckelly314/pyisotopomer: v1.0.4. Published online January 19, 2023.
884 doi:10.5281/zenodo.7552724
- 885 65. McIlvin MR, Casciotti KL. Technical updates to the bacterial method for nitrate isotopic
886 analyses. *Anal Chem.* 2011;83(5):1850-1856. doi:10.1021/ac1028984
- 887 66. McIlvin MR, Casciotti KL. Fully automated system for stable isotopic analyses of dissolved
888 nitrous oxide at natural abundance levels. *Limnol Oceanogr Methods.* 2010;8(2):54-66.
889 doi:10.4319/lom.2010.8.54
- 890 67. Scott KM, Lu X, Cavanaugh CM, Liu JS. Optimal methods for estimating kinetic isotope
891 effects from different forms of the Rayleigh distillation equation 1 Associate editor: J.
892 Horita. *Geochim Cosmochim Acta.* 2004;68(3):433-442. doi:10.1016/S0016-
893 7037(03)00459-9
- 894 68. LI W. Measurement of the absolute abundance of oxygen-17 in V-SMOW. *Chin Sci Bull.*
895 1988;33:1610-1613. Accessed June 10, 2021. <https://ci.nii.ac.jp/naid/80004607415/>
- 896 69. Santoro AE, Buchwald C, McIlvin MR, Casciotti KL. Isotopic Signature of N₂O Produced
897 by Marine Ammonia-Oxidizing Archaea. *Science.* 2011;333(6047):1282-1285.
898 doi:10.1126/science.1208239
- 899 70. Dutton GS, Elkins JW, Hall BD. Nitrous Oxide data from the NOAA/ESRL halocarbons in
900 situ program. Published online 2021. Accessed November 19, 2021.
901 <https://data.nodc.noaa.gov/cgi-bin/iso?id=gov.noaa.ncdc:C01556>
- 902 71. Röckmann T, Kaiser J, Brenninkmeijer CAM, Brand WA. Gas chromatography/isotope-
903 ratio mass spectrometry method for high-precision position-dependent ¹⁵N and ¹⁸O
904 measurements of atmospheric nitrous oxide. *Rapid Commun Mass Spectrom.*
905 2003;17(16):1897-1908. doi:10.1002/rcm.1132

- 906 72. Glover DM, Jenkins WJ, Doney SC. *Modeling Methods for Marine Science*. Cambridge
907 University Press; 2011. doi:10.1017/CBO9780511975721
- 908 73. Lorquet JC, Cadet C. Excited states of gaseous ions: I. Selection rules in photoelectron
909 spectroscopy and photoionization. The case of N₂O⁺. *Int J Mass Spectrom Ion Phys*.
910 1971;7(3):245-254. doi:10.1016/0020-7381(71)80020-7
- 911 74. Märk E, Märk TD, Kim YB, Stephan K. Absolute electron impact ionization cross section
912 from threshold up to 180 eV for N₂O⁺+e⁻→N₂O⁺⁺+2e⁻ and the metastable and collision
913 induced dissociation of N₂O⁺. *J Chem Phys*. 1981;75(9):4446-4453. doi:10.1063/1.442611
- 914 75. Bigeleisen J. Chemistry of Isotopes. *Science*. 1965;147(3657):463-471.
915 doi:10.1126/science.147.3657.463
- 916 76. Begun GM, Landau L. Metastable Transitions in N₂O⁺. *J Chem Phys*. 1962;36(4):1083-
917 1084. doi:10.1063/1.1732641
- 918
- 919

920 **Table 1.** Reference materials for N₂O isotopic analysis and intercalibration. Except for one internal standard (B6),
 921 calibrated values were provided via independent measurement by S. Toyoda, Tokyo Tech., J. Mohn, EMPA; or, in
 922 the case of tropospheric N₂O, the 2018 annual average measured at Jungfraujoch, Switzerland, reported by Yu et al.
 923 (2020). The laboratories participating in the intercalibration exercise were at Stanford University (“Lab 1”) and the
 924 University of Basel (“Lab 2”). ³¹R values represent the inherent, unscrambled ³¹R of each reference material,
 925 calculated from eqn. (6).

Reference material	Matrix	Mole fraction	$\delta(^{15}\text{N}^\alpha)$	$\delta(^{15}\text{N}^\beta)$	$\delta(^{15}\text{N}^{\text{sp}})$	$\delta(^{15}\text{N}^{\text{bulk}})$	$\delta(^{18}\text{O})$	^{31}R ($^{15}\text{R}^\alpha + ^{17}\text{R}$)	^{45}R	^{46}R	Calibration by	
		$\mu\text{mol mol}^{-1}$		(%o, vs. air N ₂)			(%o, vs. VSMOW)					
S2 reference gas	Synthetic air	90	5.55	-12.87	18.42	-3.66	32.73	0.004083	0.007712	0.002087	Toyoda & Mohn	
B6 reference gas	He	900	-0.40	-0.15	-0.26	-0.28	41.95	0.004063	0.007739	0.002106	Lab 1 internal standard	
Tropospheric N ₂ O (2018 annual average)	Air	~0.33	15.6	-2.3	17.9	6.6	44.4	0.004123	0.007787	0.002111	Yu et al. (2020)	
CA06261	Synthetic air	90	-22.21	-49.28	27.07	-35.75	26.94	0.003980	0.007475	0.002075	Toyoda & Mohn	
53504	Synthetic air	90	1.71	94.44	-92.73	48.08	36.01	0.004070	0.008093	0.002095	Toyoda & Mohn	
CA08214	Synthetic air	90	17.11	-3.43	20.54	6.84	35.39	0.004126	0.007790	0.002093	Toyoda & Mohn	
90454	Synthetic air	90	25.73	25.44	0.29	25.59	35.88	0.004158	0.007928	0.002094	Toyoda & Mohn	
94321	Synthetic air	90	50.52	2.21	48.31	26.37	35.54	0.004249	0.007934	0.002094	Toyoda & Mohn	
Lab 1 pure N ₂ O direct injection ("A01")	Pure N ₂ O	N/A	0.24	0.12	0.13	0.18	39.85	0.003734	0.007742	0.002101	Toyoda	
Lab 2 pure N ₂ O direct injection	Pure N ₂ O	N/A	-4.07	3.59	-7.66	-0.24	39.25	0.004044	0.007739	0.002100	Mohn	

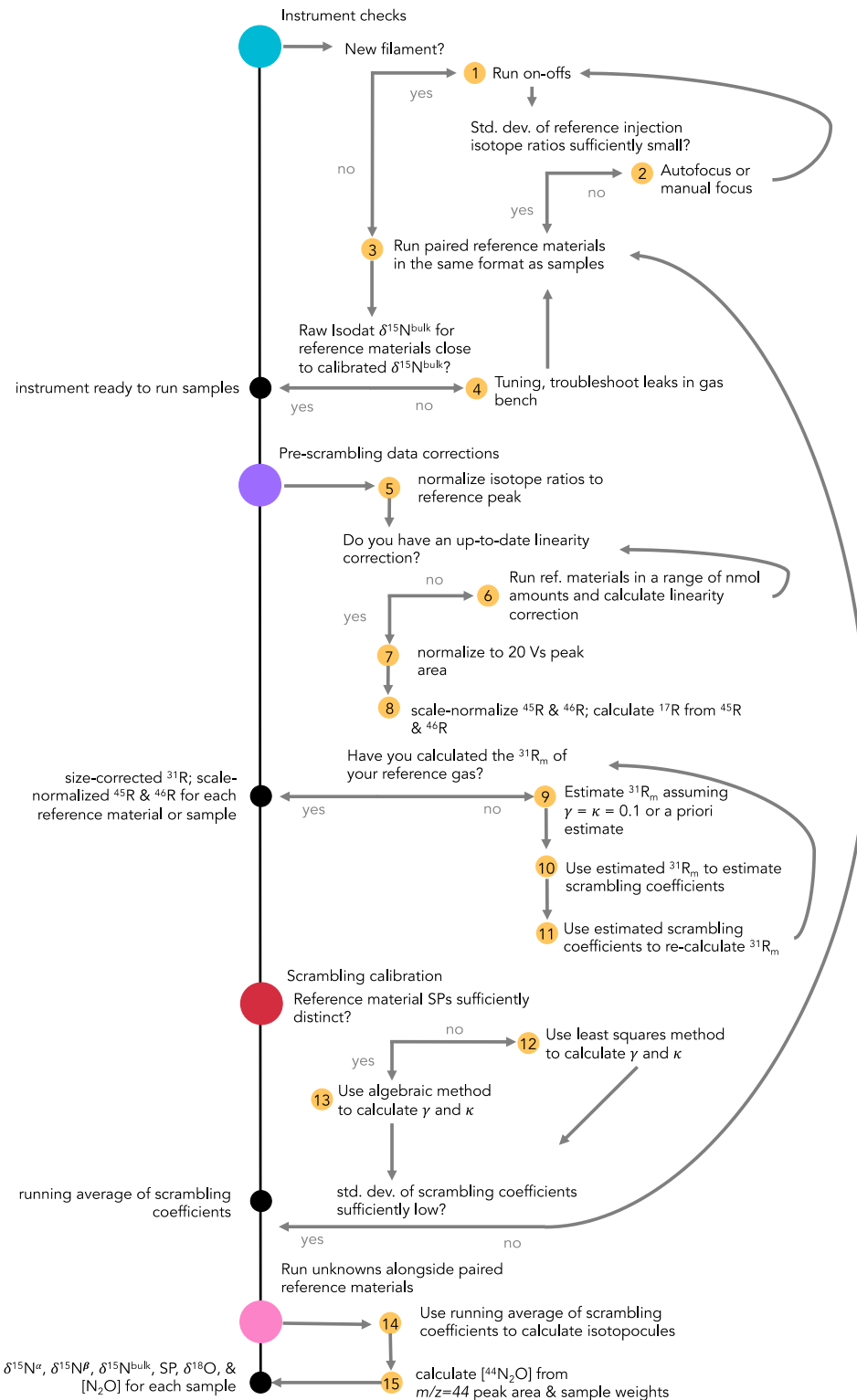
926
927

928 **Table 2.** N₂O isotopic composition of reference materials and two unknowns analyzed by two IRMS laboratories,
 929 calculated using γ and κ values determined from reference materials 53504 and CA08214 with the algebraic
 930 solution. $\delta(^{15}\text{N}^\alpha)$, $\delta(^{15}\text{N}^\beta)$, $\delta(^{15}\text{N}^{\text{sp}})$ and $\delta(^{15}\text{N}^{\text{bulk}})$ are reported in ‰ vs. Air N₂, and $\delta(^{18}\text{O})$ is reported in ‰ vs.
 931 VSMOW. Uncertainties are standard deviations of replicate bottles and do not include calibration uncertainties. The
 932 root-mean square deviation (RMSD) was calculated with respect to calibrated values.

933

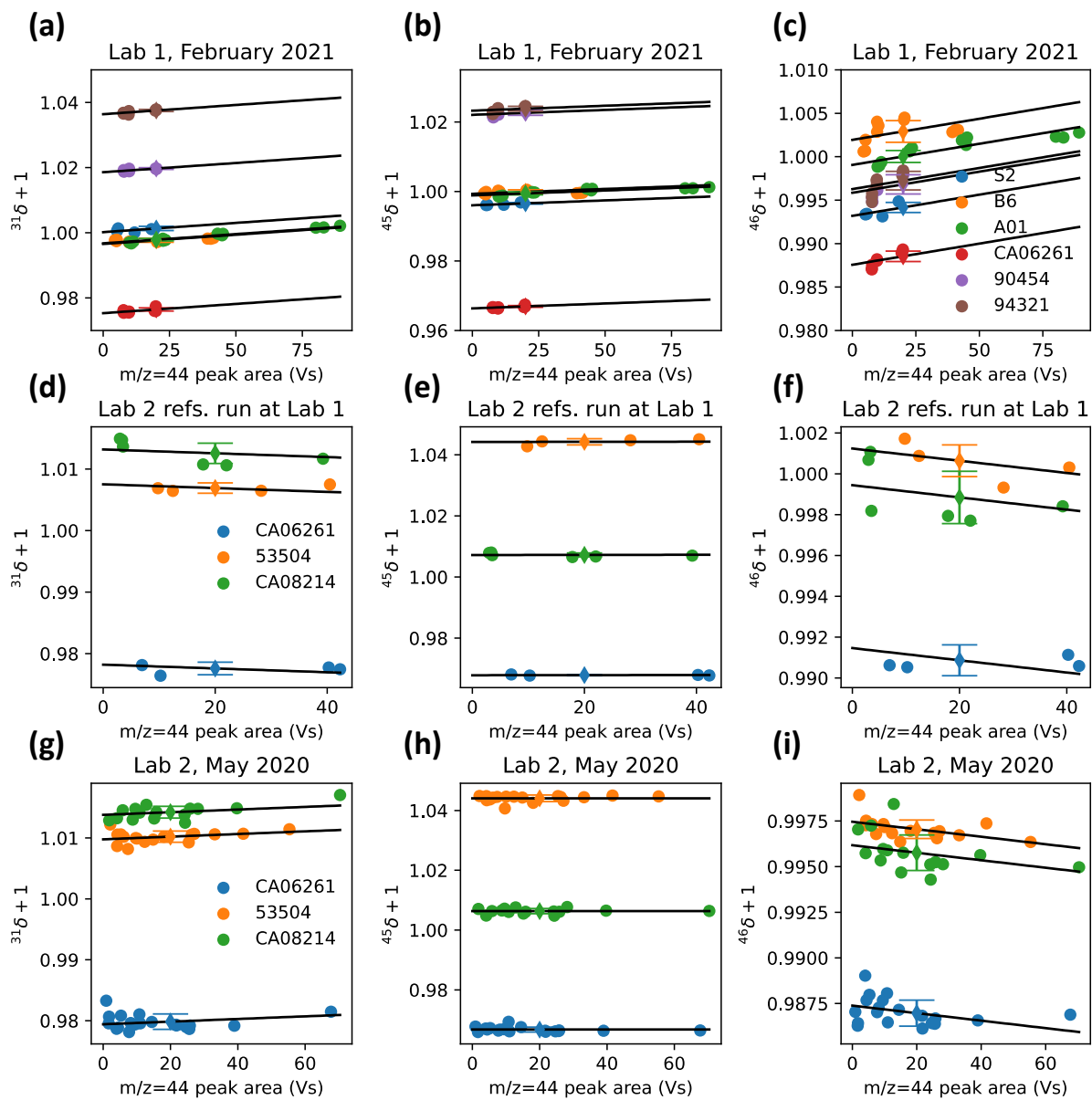
Reference material		<i>n</i>	$\delta(^{15}\text{N}^\alpha)$				$\delta(^{15}\text{N}^\beta)$				$\delta(^{15}\text{N}^{\text{sp}})$				$\delta(^{15}\text{N}^{\text{bulk}})$				$\delta(^{18}\text{O})$								
			σ	σ	σ	σ	σ	σ	σ	σ	σ	σ	σ	σ	σ	σ	σ	σ	σ	σ							
												(‰, vs. air N ₂)												(‰, vs. VSMOW)			
CA06261	Calibrated value		-22.2		-49.3		27.1		-35.7		26.9																
	Lab 1	4	-20.6	1.3	-50.5	1.3	29.9	2.7	-35.6	0.2	28.4	0.8															
	Lab 2	16	-20.5	1.4	-50.9	2.6	30.4	3.8	-35.7	1.0	27.6	1.8															
	RMSD		2.3		2.1		4.4		0.2		1.5																
53504	Calibrated value		1.7		94.4		-92.7		48.1		36.0																
	Lab 1	4	0.0	1.0	95.7	2.1	-95.7	2.5	47.9	1.1	37.6	0.8															
	Lab 2	15	1.7	1.0	94.5	1.9	-92.8	2.9	48.1	0.6	36.4	1.6															
	RMSD		1.7		1.3		3.0		0.2		1.7																
CA08214	Calibrated value		17.1		-3.4		20.5		6.8		35.3																
	Lab 1	6	17.0	2.0	-2.4	0.9	19.4	2.9	7.3	0.7	36.3	1.4															
	Lab 2	16	17.0	1.1	-3.2	0.7	20.2	1.3	6.9	0.6	36.0	3.6															
	RMSD		0.1		1.1		1.2		0.5		1.3																
Tropospheric N ₂ O	Calibrated value		15.6		-2.3		17.9		6.6		44.4																
	Lab 1	7	15.1	0.8	-2.5	2.3	17.5	2.8	6.3	1.0	43.1	2.1															
	Lab 2	2	15.8	1.1	-3.7	0.0	19.5	1.0	6.1	0.5	44.7	1.0															
	RMSD		0.6		1.4		1.7		0.6		1.3																
B6	Calibrated value		-0.4		-0.1		-0.3		-0.3		41.9																
	Lab 1	7	-2.2	0.7	1.3	1.0	-3.4	1.2	-0.4	0.7	41.5	1.6															
	RMSD		1.8		1.4		3.2		0.2		0.5																
S2	Calibrated value		5.6		-12.9		18.4		-3.7		32.7																
	Lab1	6	5.0	0.5	-13.1	1.6	18.1	1.3	-4.0	1.0	31.5	1.8															
	RMSD		0.5		0.2		0.3		0.4		1.2																
Lake Lugano, 10m	Lab 1	3	13.2	0.3	-5.6	1.2	18.8	1.5	3.8	0.4	44.6	1.2															
	Lab 2	5	14.8	1.5	-6.6	1.3	21.4	2.5	4.1	0.5	45.5	0.6															
Lake Lugano, 90m	Lab 1	3	19.2	0.5	-33.1	0.7	52.3	1.2	-6.9	0.1	56.8	0.1															
	Lab 2	2	18.5	0.8	-32.4	0.3	50.9	0.5	-6.9	0.5	55.4	1.9															

934



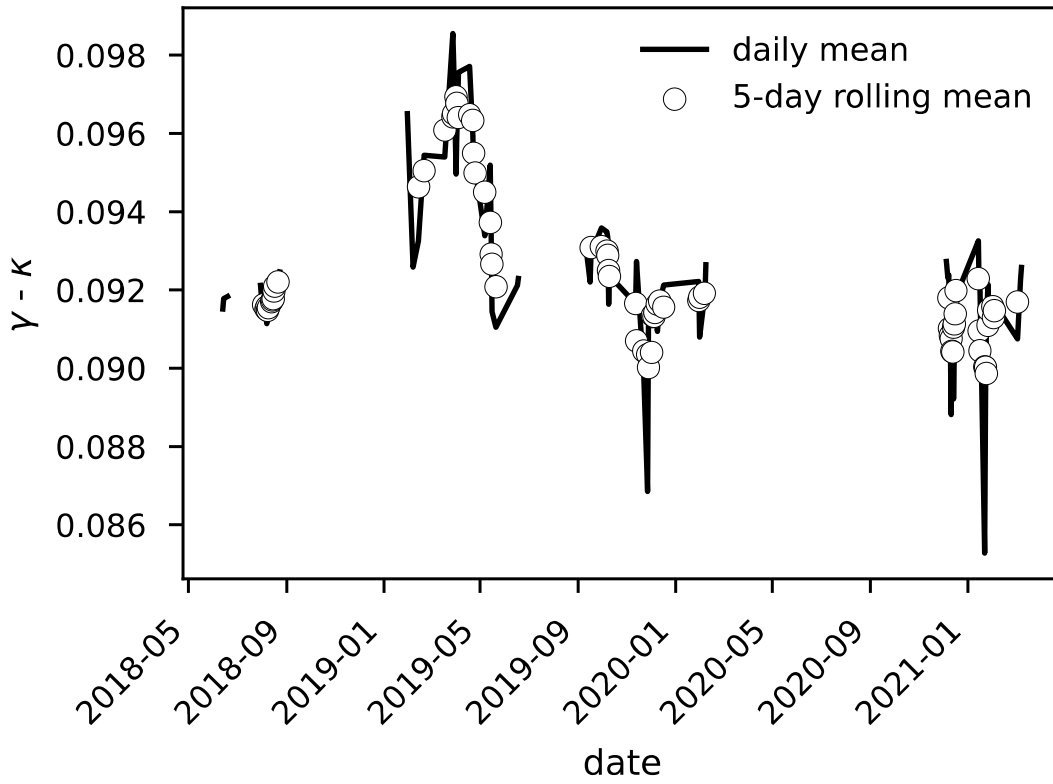
935
936
937
938
939

Figure 1. N₂O data corrections flowchart. Instrument checks, pre-scrambling data corrections, the scrambling calibration, and isotopomer calculations are laid out; numbers in yellow circles correspond to step numbers referred to in the text. Steps 1-4 are performed with raw Isodat output, steps 5-8 are accomplished in the data corrections spreadsheet template, step 9 is a simple calculation, and steps 10-14 are accomplished with the pyisotopomer code.



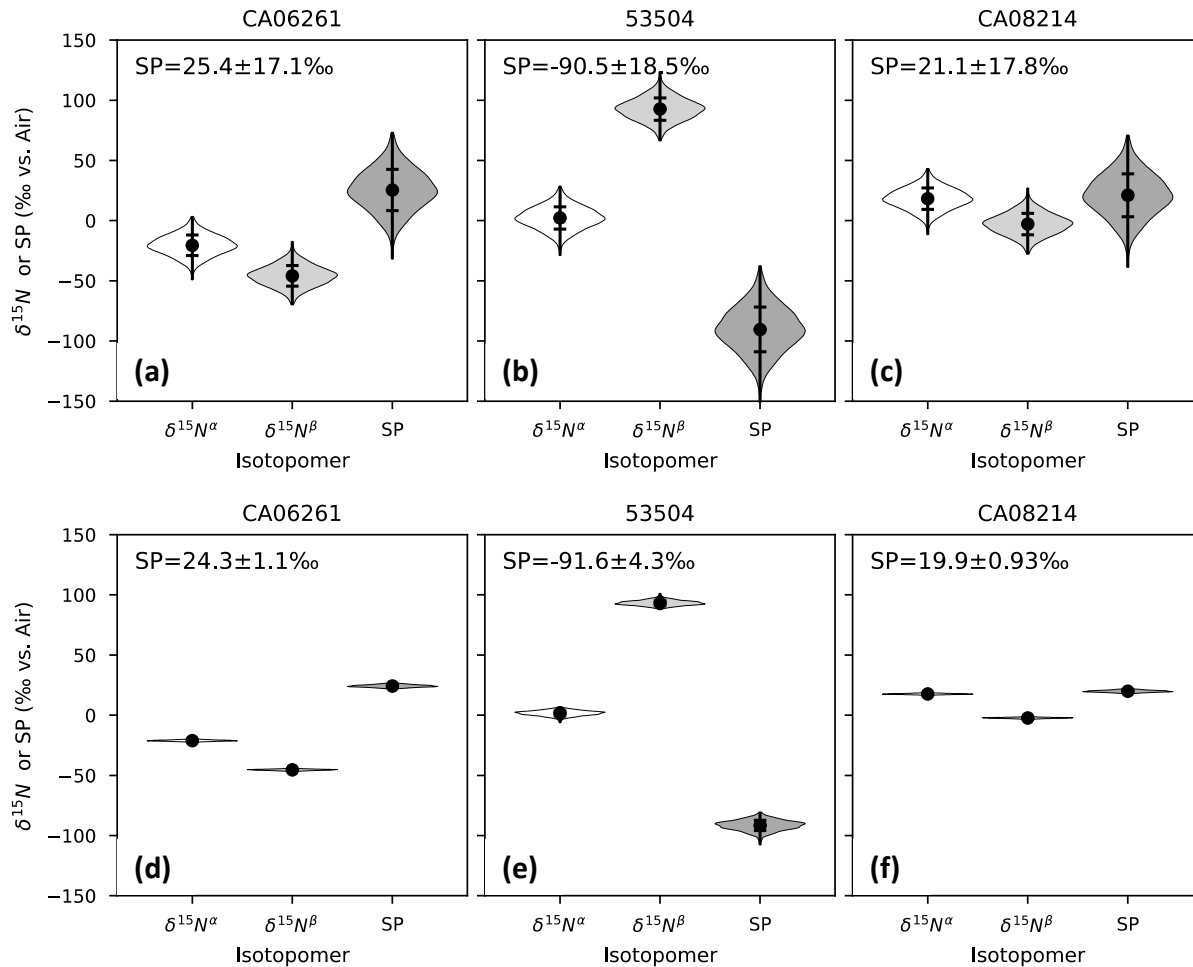
940
 941 **Figure 2.** Linearity relations for reference materials used to normalize measured isotope ratios to a peak area of 20
 942 Vs, using the dummy variable method⁶⁷. $^{31}\delta+1$ (a,d,g), $^{45}\delta+1$ (b,e,h), and $^{46}\delta+1$ (c, f, i) are plotted against m/z 44
 943 peak area. Linearity relations are shown for reference materials prepared and run in Lab 1 (a-c), reference materials
 944 prepared in Lab 2 but run in Lab 1 (d-f), and reference materials run in Lab 2 (g-i). A common slope (black line)
 945 calculated from the dummy variable method for each molecular ion ratio is overlain on each data series (colored
 946 circles). The estimated isotope ratio corresponding to a peak area of 20 Vs is also shown for each series (colored
 947 diamonds, error bars correspond to the standard error of the predicted y-value).

948



949 **Figure 3.** $\gamma - \kappa$ for the Lab 1 IRMS from June 2018 to March 2021. Daily mean $\gamma - \kappa$ (black line) values are plotted
 950 with a 5-day rolling average (dots).
 951

952



953
 954 **Figure 4.** a-c) Isotopocule values and error associated with a 10 % relative uncertainty in $\gamma - \kappa$, based on Monte
 955 Carlo simulation results, for reference materials CA062621 (a), 53504 (b), and CA08214 (c). γ and κ were modeled
 956 as random numbers centered around $\gamma = 0.174$ and $\kappa = 0.083$, with the uncertainty in $\gamma - \kappa$ equal to 10 % of the mean
 957 $\gamma - \kappa$ (0.091). d-f) Isotopocule values and error associated with a 10% relative uncertainty in the absolute values of γ
 958 $- \kappa$, holding the difference $\gamma - \kappa$ constant, for reference materials CA062621 (d), 53504 (e), and CA08214 (f). γ and
 959 κ were modeled in tandem as random numbers centered around $\gamma = 0.174$ and $\kappa = 0.083$, with uncertainties equal to
 960 10% of the mean γ , and $\gamma - \kappa$ was held constant at 0.091. Violin plots are based on a kernel density estimate of the
 961 distribution and the values plotted and reported on each figure show the mean value $\pm 1\sigma$.

962
 963